

UNCLASSIFIED  
CONFIDENTIAL

NAA-SR-9903

COPY

51 PAGES


SEP 15 1964

MASTER

## SNAP 10A REACTOR THERMAL PERFORMANCE

(Title Unclassified)

*AEC Research and Development Report*

  
This document contains restricted data as defined in the Atomic Energy Act of 1954. Its transmittal or the disclosure of its contents in any manner to an unauthorized person is prohibited.

This document contains Confidential-Restricted Data relating to civilian applications of atomic energy.

GROUP 1

*Excluded from automatic down-  
grading and declassification*



# ATOMICS INTERNATIONAL

A DIVISION OF NORTH AMERICAN AVIATION, INC.

UNCLASSIFIED  
CONFIDENTIAL

1254  
DISTRIBUTION OF THIS DOCUMENT IS UNLIMITED

## **DISCLAIMER**

**This report was prepared as an account of work sponsored by an agency of the United States Government. Neither the United States Government nor any agency Thereof, nor any of their employees, makes any warranty, express or implied, or assumes any legal liability or responsibility for the accuracy, completeness, or usefulness of any information, apparatus, product, or process disclosed, or represents that its use would not infringe privately owned rights. Reference herein to any specific commercial product, process, or service by trade name, trademark, manufacturer, or otherwise does not necessarily constitute or imply its endorsement, recommendation, or favoring by the United States Government or any agency thereof. The views and opinions of authors expressed herein do not necessarily state or reflect those of the United States Government or any agency thereof.**

## **DISCLAIMER**

**Portions of this document may be illegible in electronic image products. Images are produced from the best available original document.**



#### LEGAL NOTICE

This report was prepared as an account of Government sponsored work. Neither the United States, nor the Commission, nor any person acting on behalf of the Commission:

A. Makes any warranty or representation, express or implied, with respect to the accuracy, completeness, or usefulness of the information contained in this report, or that the use of any information, apparatus, method, or process disclosed in this report may not infringe privately owned rights; or

B. Assumes any liabilities with respect to the use of, or for damages resulting from the use of information, apparatus, method, or process disclosed in this report.

As used in the above, "person acting on behalf of the Commission" includes any employee or contractor of the Commission, or employee of such contractor, to the extent that such employee or contractor of the Commission, or employee of such contractor prepares, disseminates, or provides access to, any information pursuant to his employment or contract with the Commission, or his employment with such contractor.

Printed in USA

Price \$1.05

Available from the

U. S. Atomic Energy Commission  
Technical Information Extension,  
P. O. Box 1001  
Oak Ridge, Tennessee.

Please direct to the same address inquiries covering the procurement of other classified AEC reports.

~~CONFIDENTIAL~~  
~~UNCLASSIFIED~~

Exempt from CCRP Re-review Requirements  
(per 7/22/82 Duff/Caudle memorandum)  
HA 3/1/04

NAA-SR-9903  
SNAP REACTOR,  
SNAP PROGRAM  
M-3679 (35th Ed.)

Classification cancelled (or changed to) ~~UNCLASSIFIED~~

by authority of Bram Feldman Letter 4/17/73 Div of Class.  
by GG DTIE, date 5/24/73 Wash. D.C.

# SNAP 10A REACTOR THERMAL PERFORMANCE

(Title Unclassified)

By

P.M. MAGEE  
G.E. DUFOE  
J.D. GORDON

## NOTICE

This report was prepared as an account of work sponsored by the United States Government. Neither the United States nor the United States Atomic Energy Commission, nor any of their employees, nor any of their contractors, subcontractors, or their employees, makes any warranty, express or implied, or assumes any legal liability or responsibility for the accuracy, completeness or usefulness of any information, apparatus, product or process disclosed, or represents that its use would not infringe privately owned rights.

~~RESTRICTED DATA~~

This document contains restricted data as defined in the Atomic Energy Act of 1954. Its transmittal or the disclosure of its contents in any manner to an unauthorized person is prohibited.

This document contains Confidential-Restricted Data relating to civilian applications of atomic energy.

# ATOMICS INTERNATIONAL

A DIVISION OF NORTH AMERICAN AVIATION, INC.  
P.O. BOX 309 CANOGA PARK, CALIFORNIA

CONTRACT: AT(11-1)-GEN-8  
ISSUED: SEPTEMBER 1, 1964

~~CONFIDENTIAL~~  
~~UNCLASSIFIED~~

DISTRIBUTION OF THIS DOCUMENT IS UNLIMITED

GG



## DISTRIBUTION

### SYSTEMS FOR NUCLEAR AUXILIARY POWER (SNAP)-REACTOR SNAP PROGRAM M-3679(35th Ed. )

	No. of Copies
Aerojet-General Corporation (NASA)	6
Aerojet-General Corporation, Sacramento	1
Aerojet-General Nucleonics	1
Aeronautical Systems Division	2
Aerospace Corporation	1
Aerospace Test Wing (AFSC)	1
Air Force Surgeon General	1
Air Force Weapons Laboratory	2
AiResearch Manufacturing Company, Phoenix	1
Army Ballistic Research Laboratories	1
Army Missile Command	1
Army Nuclear Defense Laboratory	1
ARO, Inc.	1
Air University Library	1
Argonne National Laboratory	1
Army Combat Developments Command	1
Astropower, Inc.	1
Avco Corporation	1
Battelle Memorial Institute	1
Bendix Corporation (AF)	1
Brookhaven National Laboratory	1
Bureau of Naval Weapons	2
Bureau of Ships	2
Bureau of Yards and Docks	1
California Patent Group	1
Central Intelligence Agency	1
Chicago Patent Group	1
Defense Atomic Support Agency, Sandia	1
Department of the Army	1
Director of Defense Research and Engineering (OAP)	1
Edgerton, Germeshausen and Grier, Inc., Goleta	1
Foreign Technology Division (AFSC)	1
General Atomic Division	1
General Dynamics/Astronautics (AF)	1
General Dynamics/Fort Worth	1
General Electric Company, Cincinnati	1
General Electric Company (FPD)	2
General Electric Company (MSVD)	1
General Electric Company, Richland	2
General Electric Company, San Jose	1
General Electric Company, San Jose (AF)	1
General Technologies Corporation	1
Institute for Defense Analysis	1
Ion Physics Corporation	1
Jet Propulsion Laboratory	2
Johns Hopkins University (APL)	1
Lockheed-Georgia Company	1
Lockheed Missiles and Space Company	1
Los Alamos Scientific Laboratory	1
Martin-Marietta Corporation, Denver	1
Monsanto Dayton Laboratory	1
Mound Laboratory	1
NASA Ames Research Center	1
NASA Goddard Space Flight Center	2
NASA Langley Research Center	1
NASA Lewis Research Center	4
NASA Manned Spacecraft Center	1
NASA Marshall Space Flight Center	1
NASA Scientific and Technical Information Facility	3
National Aeronautics and Space Administration, Washington	2
NASA Western Operations Office	1
Naval Air Development Center	1
Naval Ordnance Laboratory	2
Naval Postgraduate School	1
Naval Radiological Defense Laboratory	1
Naval Research Laboratory	2
Naval Underwater Ordnance Station	1
Navy Marine Engineering Laboratory	1
New York Operations Office	1
New York Operations Office, Canel Project Office	1
North American Aviation, Inc., Downey	1
Nuclear Metals, Inc.	1
Office of Naval Research	2
Office of the Assistant General Counsel for Patents (AEC)	1
Office of the Chief of Engineers	1
Office of the Chief of Naval Operations	1
Office of the Chief of Naval Operations (OP-03EG)	3
Office of the Chief of Transportation	2
Phillips Petroleum Company (NRTS)	1
Pratt and Whitney Aircraft Division	4
Pratt and Whitney Aircraft Division (NASA)	1
Rand Corporation	1
Republic Aviation Corporation	1
Sandia Corporation	1
School of Aerospace Medicine	1
Union Carbide Corporation (ORNL)	1
USAF Headquarters	8
University of California, Livermore	1
Westinghouse Electric Corporation (NASA)	1
Westinghouse Electric Corporation, Lima (AF)	1
Division of Technical Information Extension	40
AI Library (Includes 2 copies to CPAO, 2 copies to AEC, Washington, 2 copies to COO)	60

# CONTENTS

	Page
I. Introduction . . . . .	9
A. SNAP 10A Power System . . . . .	9
B. SNAP 10A Reactor . . . . .	9
C. Core Power Distribution . . . . .	14
II. Flow Distribution and Pressure Drop . . . . .	15
A. Flow Through Reactor . . . . .	15
B. Core Flow Distribution . . . . .	16
C. Reactor and Core Pressure Drop . . . . .	17
III. Steady-State Performance . . . . .	19
A. Nominal Temperature Distributions . . . . .	19
B. Hot-Channel Temperatures . . . . .	22
C. Differential Fuel-Clad Expansion . . . . .	23
D. Internal Pressure in Fuel Element . . . . .	25
E. Expansion of Internal Reflectors and Grid Plates . . . . .	26
IV. Thermal Behavior During Reactor Startup . . . . .	27
A. Startup Transients . . . . .	27
B. Nominal Orbital Startup . . . . .	28
1. Startup Conditions . . . . .	28
2. Temperatures During Initial Power Transient . . . . .	30
3. Differential Fuel-Clad Expansion . . . . .	33
4. Differential Clad-Hydrogen Barrier Expansion . . . . .	35
5. Thermal Stresses in Clad and Barrier at Junction to Upper End Cap. . . . .	35
6. Thermal Stresses in Clad and Barrier at Junction to Lower End Cap. . . . .	35
C. Startup of FS-1 Ground Test System . . . . .	36
D. Off-Design Startup Conditions . . . . .	38
E. Transient Limitations Upon Startup. . . . .	40
1. Barrier Stress Limitation . . . . .	40
2. Maximum Duration of Outlet Temperature Transient . . . . .	41
References . . . . .	43
Appendices	
A - Core Materials and Physical Properties at 950°F. . . . .	45
B - Computer Codes Used in Evaluating Thermal Performance . .	46

## TABLES

	Page
1. Summary of SNAP 10A Reactor Design Parameters . . . . .	11
2. Core Flow Areas . . . . .	15
3. Calculated SNAP 10A Pressure Drop Using Superficial Uniform Velocities Based on Total Flow Area . . . . .	17
4. Radial Temperature Profiles at Steady-State Conditions . . . . .	22
5. Summary of FS-1 Startup Conditions as Functions of Source Strength . . .	38
6. Conditions of Maximum Severity Encountered During First Transient Pulse . . . . .	39

## FIGURES

1. SNAP 10A Flight System . . . . .	10
2. SNAP 10A Reactor and Shield . . . . .	12
3. Internal View of Reactor Core . . . . .	13
4. Steady-State Axial Temperature Distributions for Nominal Center Fuel Element . . . . .	20
5. Steady-State Axial Temperature Distributions for Core Average Fuel Element . . . . .	20
6. Steady-State Axial Temperature Distributions for Internal Reflector, Core Edge Fuel Element, Orificed Coolant Channel Next to Reflector, and Stagnant Edge Channel . . . . .	21
7. Steady-State Axial Temperature Distributions . . . . .	23
8. Thermal Expansion of SNAP 10A Fuel and Clad Materials . . . . .	24
9. Hoop Stress in the SNAP 10A Reactor Cladding and Long-Term Rupture Data vs Temperature . . . . .	25
10. Overall Thermal Conductance UA for SNAP 10A Reactor . . . . .	28
11. Reactor Power, Flow Rate, Inlet and Outlet Temperature During Initial Power Transient . . . . .	29
12. Radial Temperature Profiles in Center Fuel Element at 5-1/2 Inch Elevation During Initial Power Transient . . . . .	30
13. Axial Temperature Profiles in Center Fuel Element 50 Seconds After Peak Transient Power . . . . .	31
14. Average Temperatures and Axial Clearances for Core Average Element During Initial Power Transient . . . . .	32
15. Average Temperatures and Axial Clearances for Core Edge Element During Initial Power Transient . . . . .	32



## FIGURES

	Page
16. Upper End Cap and Clad Temperatures in Center Element During Initial Power Transient . . . . .	33
17. Average Internal Reflector Temperatures During Initial Power Transient . . . . .	34
18. Internal Reflector Temperatures at Time of Maximum Core Outlet Temperature . . . . .	34
19. Effect of Source Strength on Power Transient During FS-1 Startup . . . . .	36
20. Effect of Source Strength on Outlet Temperature Transient During FS-1 Startup . . . . .	37
21. Effect of Source Strength on Flow Rate Transient During FS-1 Startup . . . . .	37
22. Clad-End Cap Temperature Difference During Outlet Temperature Transients . . . . .	42
23. Maximum Rate of Change of Outlet Temperature as Function of the Duration of the Transient . . . . .	42
24. Block Diagram of TRANCORE and CORESECT Transient Temperature Codes . . . . .	48
25. CORESECT Core Thermal Model . . . . .	49

BLANK

## ABSTRACT

This report summarizes the thermal and hydraulic performance of the SNAP 10A reactor. The anticipated flow distribution and pressure drop are discussed. Nominal steady-state temperature distributions for the core average, edge, and center fuel elements are given. Maximum temperatures within the center fuel element are estimated by considering hot-channel factors, which include the effects of eccentric fuel rods, tricuspid channel geometry, and uncertainties in power and flow distributions. Thermal stresses, associated with the resulting "hot" element temperatures, are investigated. Several startup transients are analyzed; in each case, maximum temperatures and temperature gradients are determined and the resulting stresses investigated. Particular emphasis is placed upon the startup of the flight system in space.

The analysis indicates that the SNAP 10A reactor is a conservative thermal design; all temperatures and thermal stresses, during startup and steady-state operation, are well within design limits.



BLANK

## I. INTRODUCTION

### A. SNAP 10A POWER SYSTEM

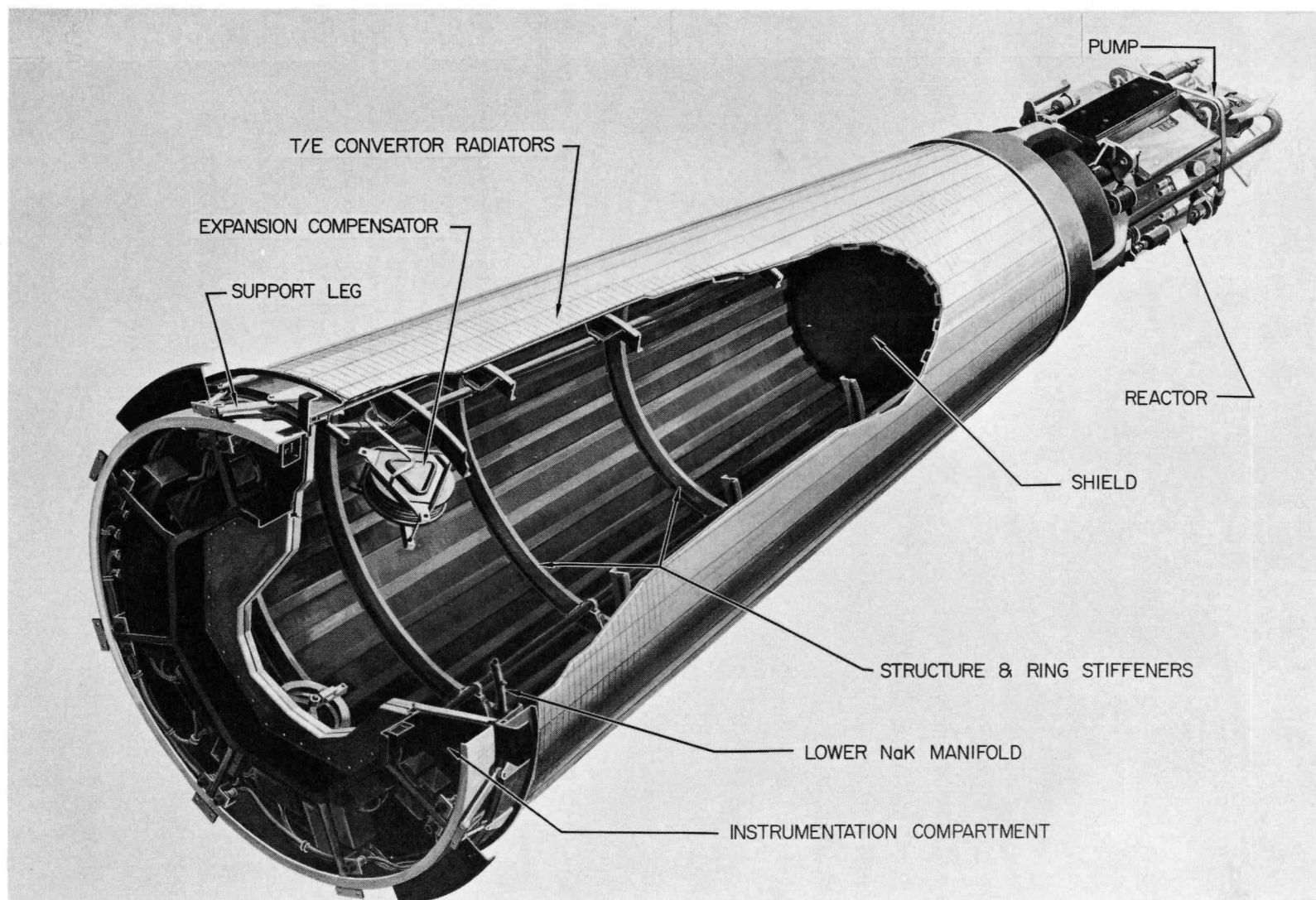
The SNAP 10A reactor is intended for use as a primary power source on satellites and other space vehicles. Generation of power in space requires a compact system with remote control capabilities, long life, high reliability, and an ability to operate in a space environment characterized by a high vacuum, meteoroid showers, and other phenomena not common to terrestrial environments.

The SNAP 10A power system (Figure 1) employs thermoelectric elements to convert the heat developed by a compact nuclear reactor into electrical energy. Circulating liquid metal (NaK-78 sodium-potassium alloy) transfers the heat generated by the reactor to the thermoelectric elements. Electrical power is generated as a result of the heat transfer through the elements with heat rejection to space. SNAP 10A system details and operation are described in detail in Reference 1, and a summary of design parameters is given in Table 1.

The reactor subsystem (Figure 2) includes the reactor vessel, beryllium external reflector structure, reactor support legs, thermoelectric pump, and radiation shield. Active reactor control is effected by four movable drums in the reflector assembly. These drums are used only during reactor startup, steady-state control being passive, that is, based on the inherent negative temperature coefficient of the reactor. The radiation shield, located directly below the reactor, protects the electronic hardware within the instrumentation compartment.

### B. SNAP 10A REACTOR

The SNAP 10A reactor core (Figure 3) is composed of 37 moderator-fuel elements. These elements are arranged in a triangular array, on 1.26-in. centers, to form a core which is hexagonal in cross section. The overall dimensions of the active core are 8.750 in. across corners, approximately 8 in. across flats, and 12.250 in. in length. The core assembly is contained within a cylindrical reactor vessel of Type-316 stainless steel. The vessel has an internal diameter of 8.875 in., is 16 in. in length, and has a minimum wall thickness of 0.032 in. Internal side reflectors of beryllium are used to round out the hexagonal core configuration and fill the void spaces in the core vessel.



9-13-62

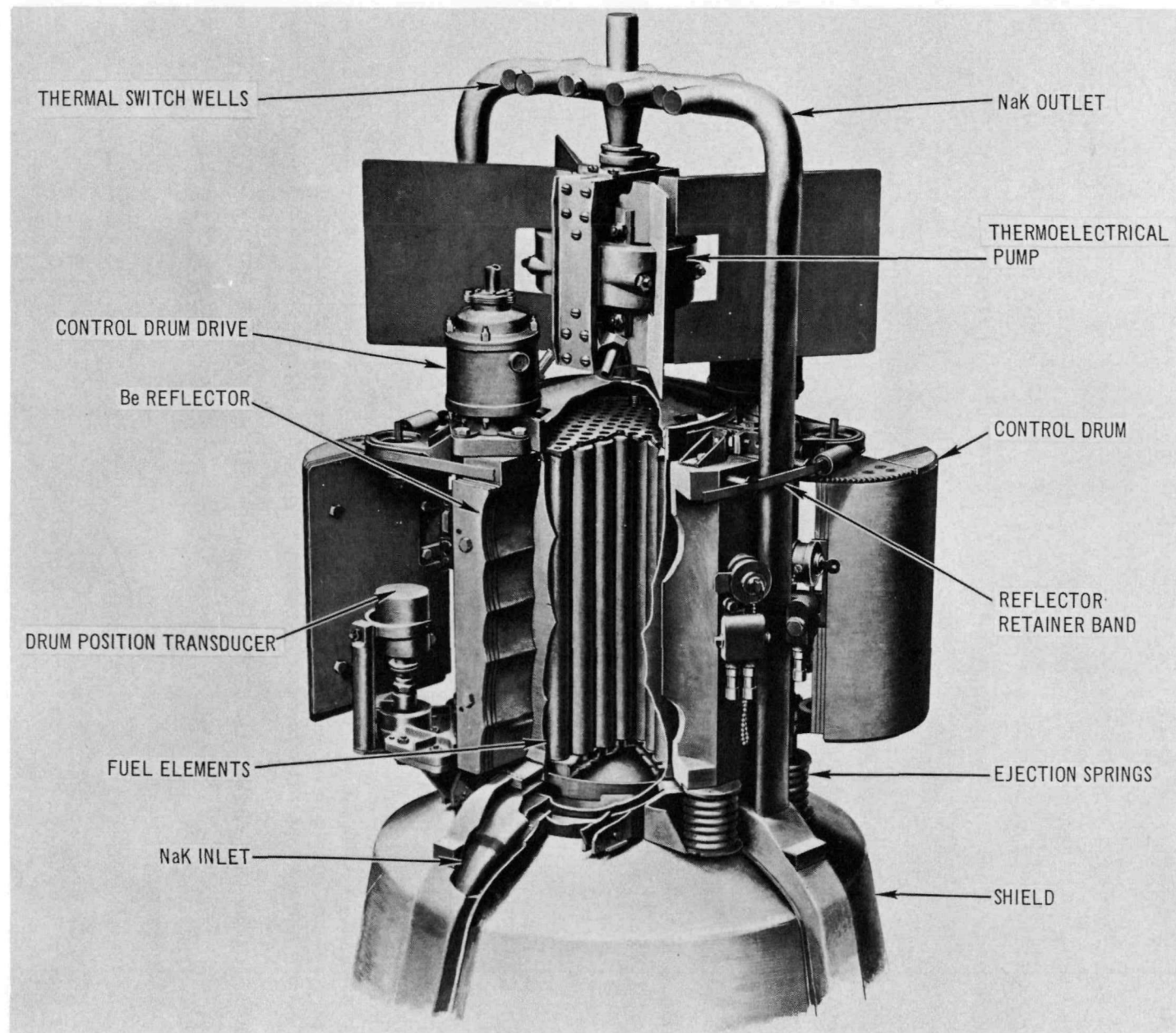
7561-0033C

Figure 1. SNAP 10A Flight System



TABLE 1  
SUMMARY OF SNAP 10A REACTOR DESIGN PARAMETERS

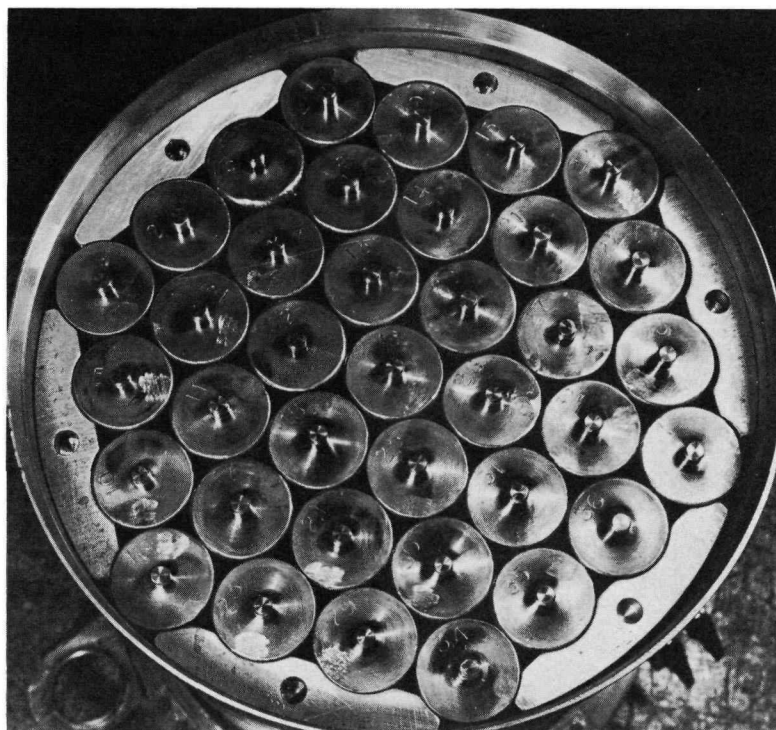
Operating Conditions	
Reactor power — average (kwt)	34
Net electrical power from system — minimum (watts)	500
Operating lifetime (yr)	1.0
Reactor inlet temperature (°F)	900
Reactor outlet temperature (°F)	1010
NaK flow rate (lb/hr)	4920
Core Parameters	
Core radial peak/average power factor	1.31
Core axial peak/average power factor	1.47
Fuel element peaking factor	1.00
Number of fuel elements	37
Number of internal reflectors	6
Total active heat-transfer area in core (ft <sup>2</sup> )	12.35
Nominal heat-transfer coefficient (Btu/hr-ft <sup>2</sup> °F)	1500
Nominal core pressure (psia)	5
Minimum core pressure (psia)	2
Maximum core pressure (psia)	10
Calculated reactor pressure drop (psi)	0.168
Maximum fuel temperature (°F)	1082
Maximum clad surface temperature (°F)	1061
Core Dimensions (in inches)	
Fuel element pitch (triangular arrangement)	1.260 ± 0.003
Fuel element diameter (cladding OD)	1.25 ± 0.002
Clad thickness	0.015 ± 0.0005
Fuel length	12.25 ± 0.002
Diffusion barrier thickness	0.003 ± 0.001
Diametric fuel-barrier clearance	0.004 ± 0.0005
Fuel diameter	1.212 ± 0.0005
ID of coated cladding	1.214 ± 0.001



5-17-62

Figure 2. SNAP 10A Reactor and Shield

7580-10512Ca



7-5-63

7561-0516

Figure 3. Internal View of Reactor Core

The reactor fuel is a hydrided zirconium-uranium alloy containing 10 wt % uranium and is hydrided to a nominal  $N_H$  of 6.35 ( $6.35 \times 10^{22}$  atoms of hydrogen/ $\text{cm}^3$  of fuel). The fuel is formed into rods of 1.21-in. diameter and 12.25-in. length and is canned in Hastelloy-N cladding tubes. Internal surfaces of the cladding tubes are coated with a 3.0 mil layer of ceramic glass material. This coating acts as a hydrogen barrier for the fuel. Each fuel element weighs 3.4 lb and has an overall length of 12.82 in.

The elements are positioned in the vessel between grid plates of Type-316 stainless steel. End pins, 0.242 and 0.180 in. in diameter, engage holes in the upper and lower grid plates, respectively, to position the elements in the core. The lower grid plate is supported by a ring at the bottom of the reactor vessel. The top grid plate is spring-loaded against the vessel top head to permit thermal expansion of the core in the axial direction.

All coolant flow within the core is through the interstices formed by adjacent fuel elements or by elements and the internal side reflectors. The orifice plate located below the lower grid plate was intended to produce the desired



flow distribution: equal coolant temperature rise in all coolant channels and a constant outlet temperature profile across the core. The coolant plenum chambers, above and below the core assembly in the vessel, provide mixing space for the coolant.

### C. CORE POWER DISTRIBUTION

Because of the geometric symmetry of the 10A core and reflector, radial and axial power distributions are expected to be symmetrical about the core center. Local power peaking around the fuel elements is expected to be negligible. There is no significant reflector peaking in either the axial or radial plane. Because of small fractional burnup of fuel and resultant small control system movement, little change of core power profiles is expected during the design life of the reactor. For purposes of analysis, axial and radial power distributions can be represented by the following expressions:

- 1) Axial Power Distribution — Normalized to an average axial power generation rate of 1.0.

$$P(z) = 1.47 \cos (1.48 - 0.241 z) \quad 0 < z < 12.25 \text{ in.}$$

- 2) Radial Power Distribution — Normalized to an average radial power generation rate of 1.0.

$$P(r) = 1.31 \cos (0.244 r) \quad 0 < r < 4.03 \text{ in.}$$

## II. FLOW DISTRIBUTION AND PRESSURE DROP

### A. FLOW THROUGH REACTOR

The NaK coolant enters the reactor via two diametrically opposed inlet nozzles located below the lower grid plate. The velocity of entry into the lower plenum is 3.2 ft/sec in a direction normal to the reactor axis. Within the lower plenum, the flow decelerates and turns to enter the core. The coolant first passes through the lower grid plate assembly: an orifice plate and a support plate, separated by 0.380 in. The orifice plate contains 72 holes which correspond in location to 72 flow passages within the core. The holes vary in diameter from 3/16 in. to 1/4 in. in steps of 1/64 in. The largest holes are in the center of the orifice plate, and the size of the holes diminishes as the distance from the center of the plate increases. After passing through the orifice plate, the coolant enters the core through seventy-two 3/8-in. holes in the support plate.

The core flow area is composed of the 72 orificed coolant channels and 12 unorificed channels at the periphery of the core. The peripheral channels receive flow only by crossflow from the interior channels. Each tricus channel formed between three fuel elements has a hydraulic diameter of 0.151 in. while, because of the smaller edge channels, the core average hydraulic diameter is 0.142 in. As shown in Table 2, the total core flow area is 6.04 in.<sup>2</sup>.

TABLE 2  
CORE FLOW AREAS

	Number	Hydraulic Diameter (in.)	Total Flow Area (in. <sup>2</sup> )
Tricus channels	54	0.151	3.987
Side channels	18	0.075	1.118
Unorificed peripheral channels	12	0.100	0.935
Total core flow area (in. <sup>2</sup> )			6.04
Area of openings in orifice plate (in. <sup>2</sup> )			2.60
Area of openings in baffle plates*(in. <sup>2</sup> )			7.96

\*The support plate and upper grid plate are herein referred to as baffle plates.

The coolant leaves the core through seventy-two 3/8-in. diameter holes in the upper grid plate. In the upper plenum, the flow converges to the outlet nozzle in the center of the top head, and leaves the reactor at a velocity of 8.2 ft/sec.

## B. CORE FLOW DISTRIBUTION

Ideally, the core flow distribution would match the radial power distribution, and the coolant temperature rise in each channel would be identical. However, this ideal distribution has not been achieved because of:

- 1) Mixing between the lower orifice plate and support plate
- 2) Crossflow within the core
- 3) Nonuniform velocity distribution in plenums.

The flow distribution in a reactor is dictated by the flow passages which have the largest fractions of the total pressure drop. If shaping of the flow distribution is desired, the device which does the shaping should consume more of the overall pressure drop than do other incidental sources of head loss. When the pressure drop across an orifice plate is only 13% of the total reactor pressure drop, as it is in SNAP 10A, it should not be expected that the core velocity profile will conform closely to the profile for which the orifice plate was designed.

Circumferential or tangential variations in flow rate are induced by the non-symmetric introduction of coolant at the entrance to the reactor. Near the top of the core, the flow will converge towards the reactor outlet line. Convergence can start in the core, by crossflow, before the flow reaches the upper plenum. Although these effects have not been experimentally measured, they are suspect because the reactor entrance and exit losses constitute 78% of the total reactor pressure drop. It is expected that by the time the time the coolant has traversed half the length of the core, the flow distribution will be nearly uniform.

The importance of the core flow distribution upon fuel element temperatures can be assessed by a comparison of two limiting cases. First, in an ideally orificed SNAP 10A core, where the coolant flow profile exactly matches the radial power profile, the maximum fuel temperature would be 1048°F. Second, if no orificing were provided and the velocity profile was uniform, the maximum fuel temperature in the center fuel element would be 1078°F. (These



temperatures are based on an inlet coolant temperature of 900°F.) This indicates how small an improvement can be achieved by perfect orificing of the SNAP 10A reactor, and, conversely, the effect that a 21% flow deficiency would have on fuel temperatures. Since the higher of the two temperatures is well below current temperature limits, and since the ideal flow distribution will not be achieved, much of the SNAP 10A analysis is based on the higher temperatures attained in a fuel element surrounded by flow-deficient channels; i.e., a uniform radial flow distribution is assumed throughout the core.

### C. REACTOR AND CORE PRESSURE DROP

Core pressure drop is made up of a fluid friction loss in the coolant channels plus orifice losses in the openings of the orifice plate and the two support plates. In spite of the fact that the core is orificed, the pressure drop can be approximated by using superficial uniform velocities based on the total flow areas. Velocities are based on a reactor flow rate of 82 lb/min. Pressure drops are based on a smooth tube friction factor and a pressure-loss coefficient of 1.73 for submerged, square-edged orifices.

TABLE 3  
CALCULATED SNAP 10A PRESSURE DROP USING SUPERFICIAL  
UNIFORM VELOCITIES BASED ON TOTAL FLOW AREA

Reactor Component	Flow Area (in. <sup>2</sup> )	Velocity (ft/sec)	Pressure Drop (psi)
Reactor inlet nozzle (2 req.)	1.29	3.22	0.054
Baffle plates (2 req.)	7.96	0.532	0.005
Orifice plate	2.60	1.60	0.023
Coolant channels	6.04	0.70	0.010
Reactor outlet nozzle	0.52	8.2	<u>0.076</u>
Total for reactor			0.168

The reactor entrance and exit losses are based on 1.00 and 0.23 velocity head losses for sudden expansion and contraction, respectively. Since these two losses make up 78% of the total pressure drop, accuracy in the total figure must suffer due to inexact knowledge of entry and exit coefficients. Even though the other losses are more uncertain, they are only a minor portion of the total pressure drop.

BLANK

### III. STEADY-STATE PERFORMANCE

#### A. NOMINAL TEMPERATURE DISTRIBUTIONS

Axial profiles of the fuel centerline, fuel surface, barrier and coolant temperature are shown in Figure 4 for the core center element and in Figure 5 for the core average element. The core-edge-element mean fuel temperature, the mean internal reflector temperature, and the non-orificed outer channel coolant temperature are plotted in Figure 6. Temperatures shown in Figures 4 through 6 are "nominal" or "most probable" values and do not include hot-channel uncertainty effects.

The highest fuel element temperatures and temperature gradients are attained in the core center element. If, as assumed, the flow rates in all coolant channels are equal, the center element will also produce the highest temperature rises in the adjacent coolant channels. This would not be true for a perfectly orificed core in which the coolant temperature rise would be the same in all channels.

The maximum fuel temperature is 1078°F and occurs 8.0 in. from the core inlet in the center element. The maximum barrier temperature of 1051°F occurs on the center element near the upper end of the core. As indicated in Figure 4, the major thermal resistances are offered by the fuel and the gas gap between the fuel and the ceramic hydrogen barrier.

The calculations of the core-edge-element temperatures assume stagnant NaK in the unorificed outer channel adjacent to the element. If flow occurs in the outer channel (due to crossflow from the orificed channels), the core-edge-element fuel temperatures will be somewhat lower. The relatively flat axial temperature distributions within the internal reflector and the stagnant channel are due to the high conductivity of the beryllium reflector.

Radial temperature profiles for the center and average fuel elements are presented in Table 4. The profiles are taken at three axial positions: 4.3 in., 8.0 in., and 11.64 in. above the core inlet. The second axial position is the location of the maximum fuel temperature, and the third position is the location of the maximum barrier temperature.

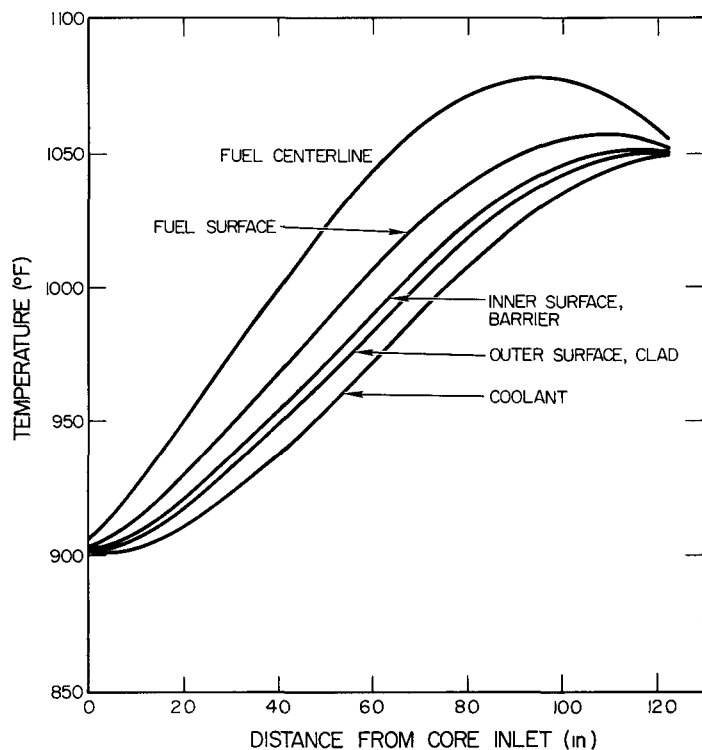


Figure 4. Steady-State Axial Temperature Distributions for Nominal Center Fuel Element

6-16-64

7623-0362

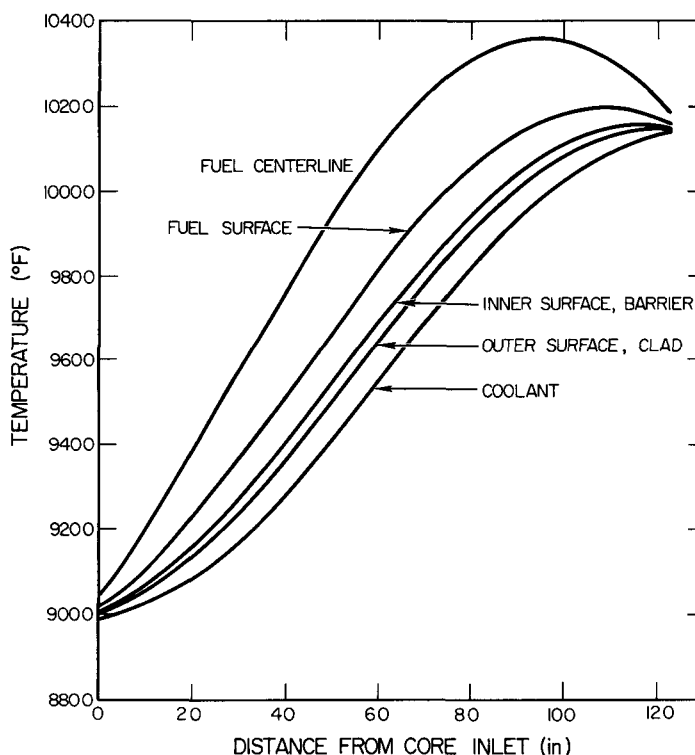
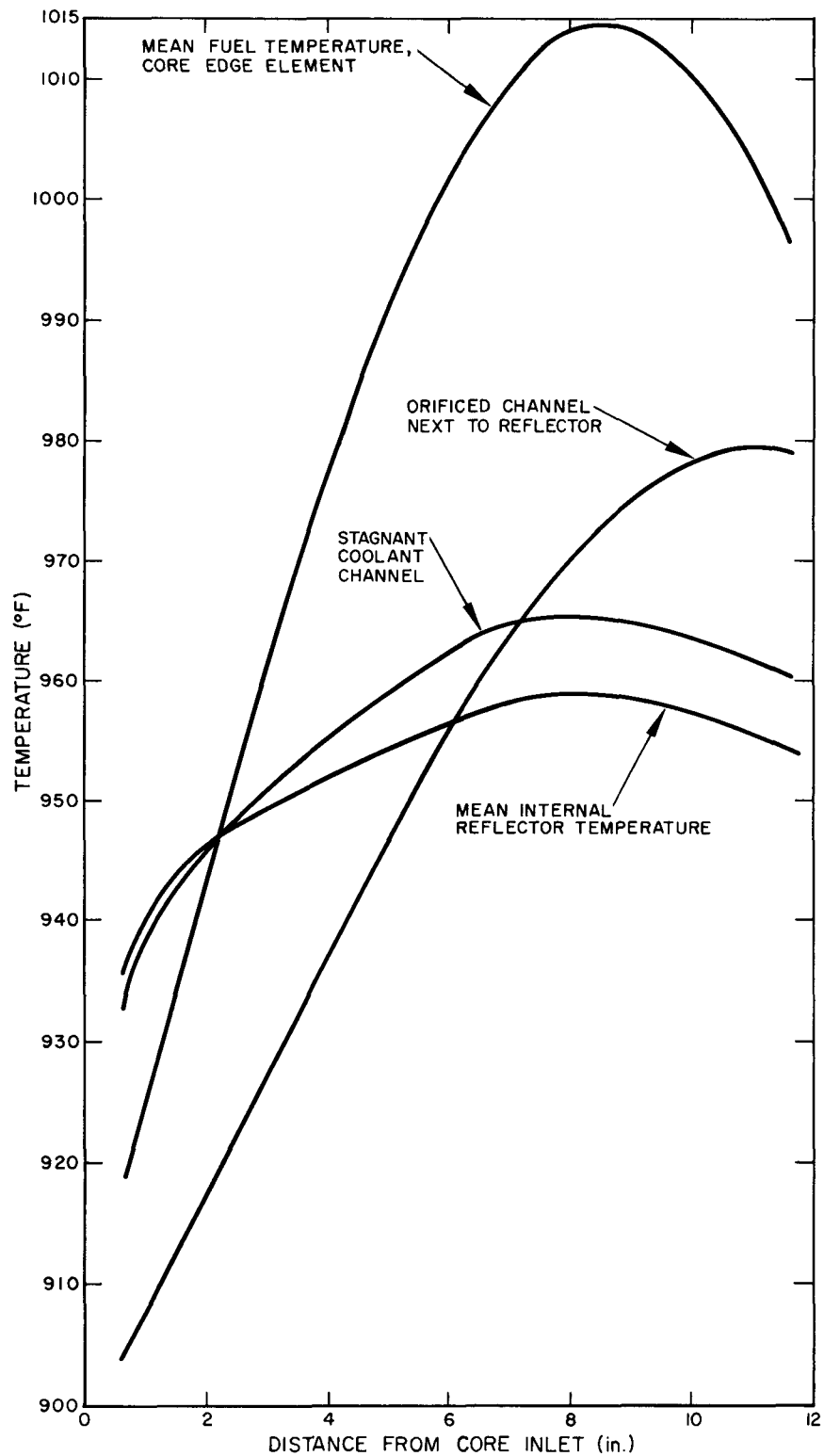


Figure 5. Steady-State Axial Temperature Distributions for Core Average Fuel Element

6-16-64

7623-0363



6-16-64

7623-0364

Figure 6. Steady-State Axial Temperature Distributions for Internal Reflector, Core Edge Fuel Element, Orificed Coolant Channel Next to Reflector, and Stagnant Edge Channel



TABLE 4  
RADIAL TEMPERATURE PROFILES  
AT STEADY-STATE CONDITIONS

Core Centerline Element										
Distance from Inlet (in.)	Fuel Element Radius (in.)									
	0.0 (centerline)	0.203	0.326	0.425	0.504	0.572	0.606 Mean Gas	0.6085 Mean Barrier	0.6175 Mean Clad	NaK
4.29	1006	1002	996	989	982	975	962	953	953	941
7.96	1070	1066	1060	1053	1047	1040	1028	1019	1018	9007
11.64	1056	1056	1055	1054	1052	1051	1049	1046	1046	1043

Core Average Element										
4.29	982	979	974	969	964	958	948	941	941	931
7.96	1029	1027	1023	1018	1013	1008	997	990	990	981
11.64	1023	1022	1021	1019	1018	1017	1014	1012	1012	1009

#### B. HOT-CHANNEL TEMPERATURES

Four basic hot-channel factors are considered in calculating 10A hot-channel temperatures:

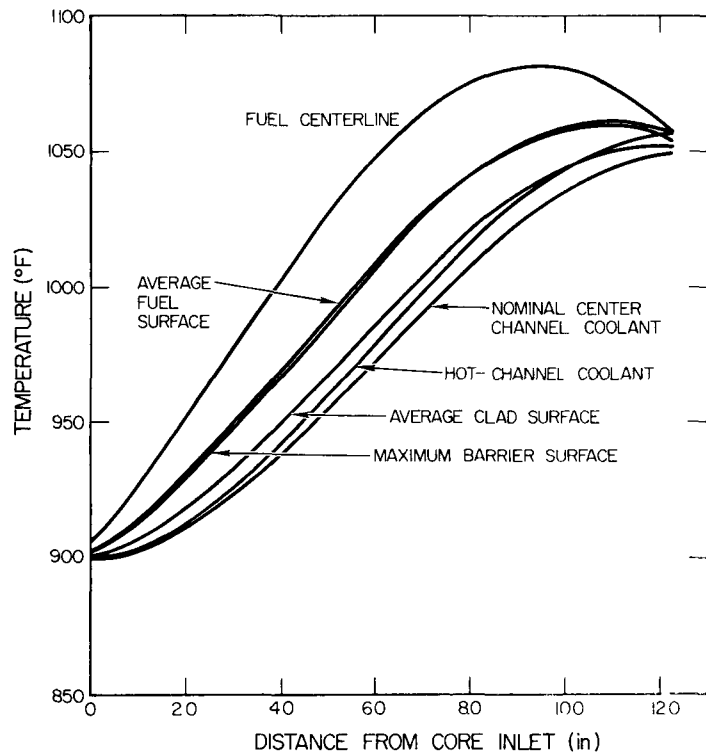
- 1) Three percent excess power is produced in the core center (hot) element. This excess is due to uncertainties in the fuel loading and in the axial and radial power distributions.
- 2) The flow rates in all tricusp coolant channels are equal. This implies a 21% flow deficiency in the center (hot) channel as compared to matched radial power and flow profiles.
- 3) The thermal conductance to the hot channel is increased 20% above nominal. This corresponds to the fuel rod in the center element and one of the other two elements bordering the hot channel being eccentric towards the hot channel. The probability of all three neighboring fuel rods being eccentric towards the hot channel is negligible. Although a three-point contact between an eccentric fuel rod and its clad is most probable (i.e., at top and bottom on one side and center on the opposite side), the more severe condition of a line contact along the length of an element was assumed.

- 4) The average heat transfer coefficient of  $1500 \text{ Btu/hr-ft}^2\text{°F}$  was reduced 50% to obtain the minimum effective local heat transfer coefficient to approximate the effect of coolant stagnation within the cusps of the channels and the local increase in clad temperature due to neighboring fuel rods.

These four hot-channel factors are considered simultaneously to produce maximum temperatures within the center fuel element. The resulting axial temperature profiles for the hot element are shown in Figure 7. The maximum fuel temperature is  $1082\text{°F}$  compared to the nominal center element maximum of  $1078\text{°F}$ , and the maximum barrier temperature is  $1061\text{°F}$  compared to the nominal maximum of  $1051\text{°F}$ .

### C. DIFFERENTIAL FUEL-CLAD EXPANSION

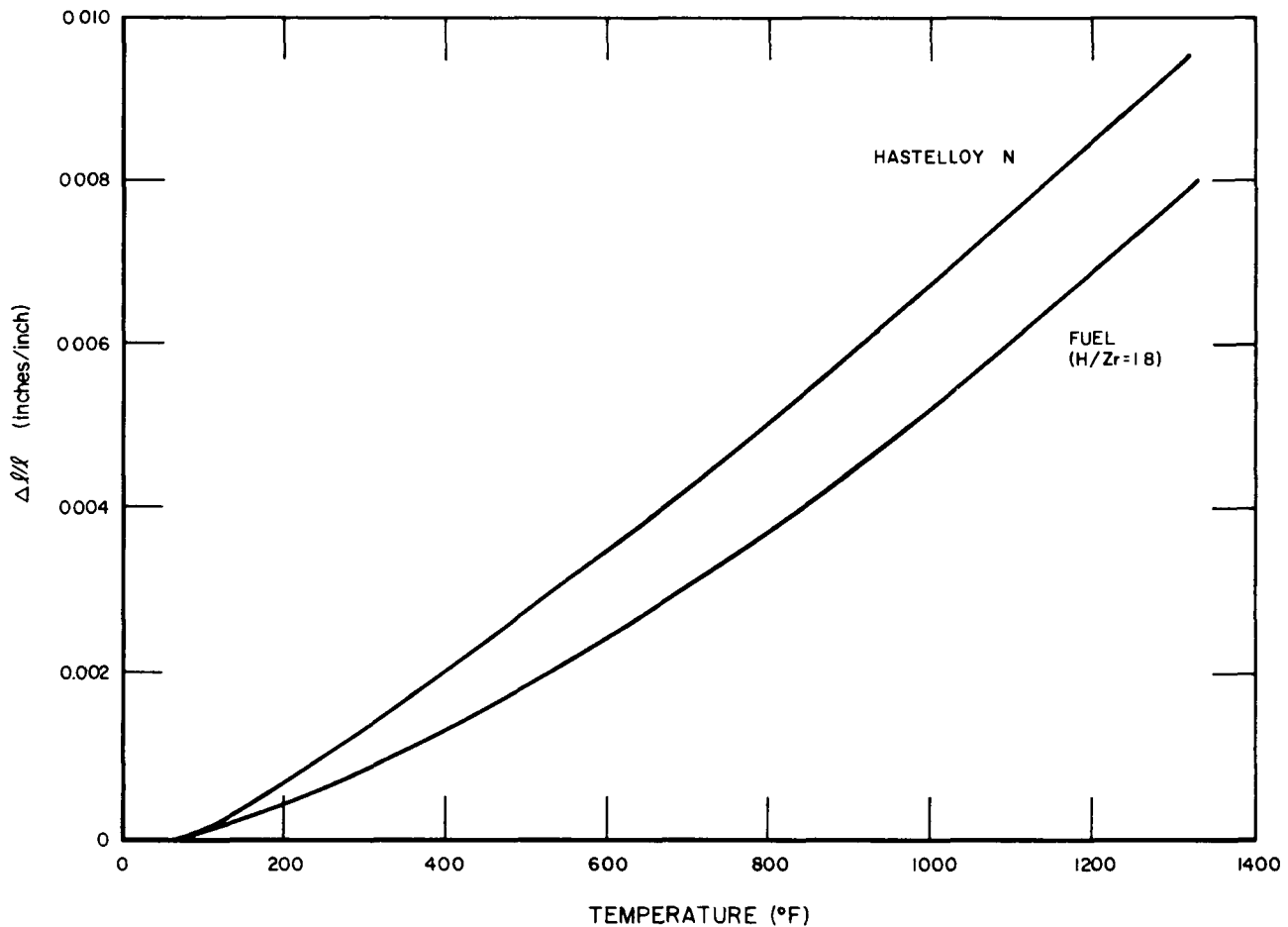
Thermal expansion data for the fuel and clad are illustrated in Figure 8. The clad material is shown to expand more rapidly than does the fuel; the Hastelloy-N exhibits 29% more thermal growth between  $70$  and  $1000\text{°F}$ .



6-16-64

7623-0365

Figure 7. Steady-State Axial Temperature Distributions



7-10-63

7623-0003

Figure 8. Thermal Expansion of SNAP 10A Fuel and Clad Materials

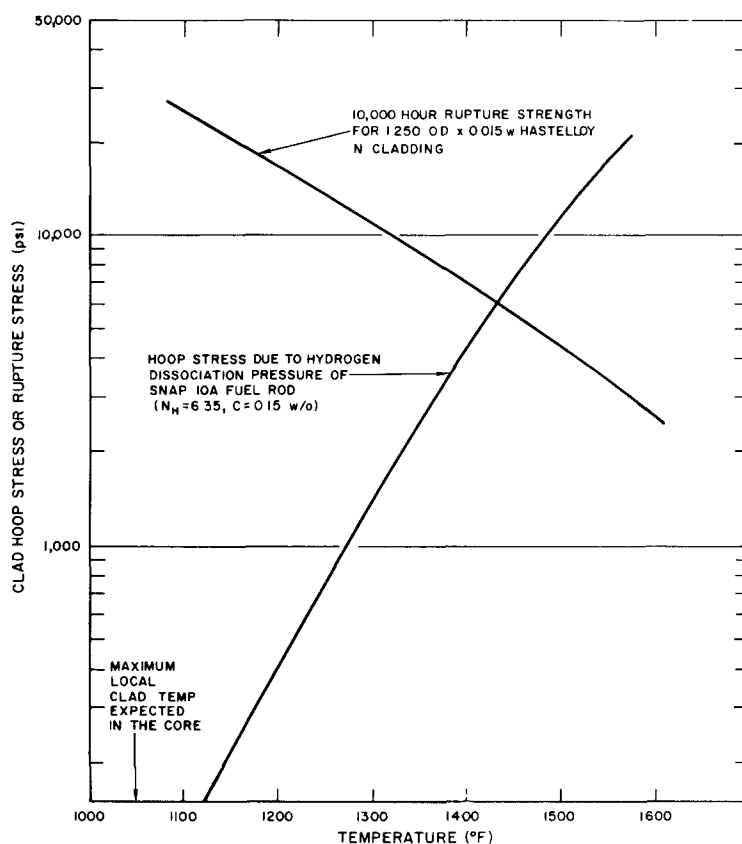
As a basis for evaluating the minimum clearances during operation, the minimum clearances at assembly were chosen. Combination of the fuel diameter and the coated tube inside diameter (with their tolerances) yields a minimum diametric assembly clearance of 0.0035 in. The minimum axial clearance before welding of the end cap is zero.

At the point of maximum fuel temperature in the center fuel element, the minimum steady-state diametric clearance between the fuel surface and the clad ID is 0.0015 in. greater than the clearance at assembly. Between room temperature and full power operation, the axial clearance (as determined by the fuel and clad temperatures averaged along the length of the center fuel rod) increases by 0.0159 in.

#### D. INTERNAL PRESSURE IN FUEL ELEMENT

The principal mechanism of pressure buildup inside the fuel elements is the dissociation pressure of uranium-zirconium-hydride in equilibrium with gaseous hydrogen. Tangential stress in the clad, due to dissociation, is plotted against temperature in Figure 9 for fuel with an  $N_H$  of 6.35 and 0.15 wt % carbon additive. A conservative approach to internal pressure evaluation is to assume that the local pressure exerted on the clad is a function of the local fuel temperature (no hydrogen redistribution). Stress rupture data for Hastelloy-N sheet were extrapolated to 10,000 hr and are illustrated in Figure 9.

Comparison of the stress level with the ultimate strength of the clad shows that the maximum allowable clad temperature is 1430°F. Maximum expected clad temperature in the SNAP 10A core is 1061°F. Therefore, excessive creep of the clad due to internal hydrogen pressure is not a limiting consideration for SNAP 10A conditions.



10-4-63

7623-0009

Figure 9. Hoop Stress in the SNAP 10A Reactor Cladding and Long-Term Rupture Data vs Temperature

NAA-SR-9903

## E. EXPANSION OF THE INTERNAL REFLECTORS AND GRID PLATES

Due to the high thermal conductivity of beryllium and the high heat-transfer coefficients in the core, the internal reflectors will operate at temperatures close to those of the adjacent coolant (Figure 6.). Axial expansion of the reflector between 70 and 950°F amounts to 0.107 in. compared to the fuel element expansion of 0.075 in.

The lower grid plate, composed of the baffle and orifice plates, will operate at a uniform temperature of approximately 900°F. No significant thermal stresses are induced in these plates.

The upper grid plate will have a radial temperature distribution matching the core outlet temperature profile. For an ideally orificed core, the outlet temperatures would be the same for all coolant channels. If a completely uniform velocity profile were to exist, channel outlet temperatures would vary by 80°F, with the center of the plate operating hotter than the periphery. This gradient produces compressive stress in the center of the plate and tensile stress at the edges, both of which are less than 8000 psi. This is below the yield stress for Type-316 stainless steel at 1000°F, the 1% creep in 10,000 hr. limit, and will not buckle the plate.



## IV. THERMAL BEHAVIOR DURING REACTOR STARTUP

### A. STARTUP TRANSIENTS

Orbital startup of the 10A reactor is effected by inward rotation of the four reflector control drums. Upon a command signal from ground, two drums are snapped in to their operating position. The other two drums are then stepped in at a nominal rate of  $0.5^\circ$  every 150 sec. The drum steps continue until a temperature sensing device on the reactor outlet line records a coolant temperature of  $1010^\circ\text{F}$ , at which time drum rotation is stopped: active control is maintained for 3 days. If, during this period, the reactor outlet temperature falls below  $1010^\circ\text{F}$ , an additional drum step will be taken to insert approximately 3 cents of reactivity. After 3 days, active control is discontinued and the reactor power and temperature follow the inherent reactivity changes within the reactor.

Four distinct periods of operation are discernible during startup: approach to criticality and sensible heat, first penetration of power range, ascent to operating temperatures, and active control at operating conditions. The reactor will go critical approximately 6 hr after rotation of the fine control drums is begun. Soon after criticality (approximately 20 min) enough energy is generated within the reactor to produce temperature increases. These mark the point of sensible heat. The first penetration into the power range follows immediately. This period of time is characterized by a peaking of the reactor power followed shortly by rapid increases in reactor outlet temperature and flow rate. The initial power transient produces the largest temperature gradients, and, consequently, the most severe thermal stresses during startup. The initial transient is followed by one or more weak secondary transients and a gradual increase in reactor temperatures to operating conditions. When the reactor outlet temperature reaches  $1010^\circ\text{F}$ , drum rotation is terminated and the active control period begun.

The stresses induced during the initial power transient are functions of the source level encountered in orbit and the fine control drum stepping rate. In addition, the nuclear and thermal characteristics of the core (e.g., fuel and grid plate temperature coefficients, heat-transfer coefficient, fuel thermal conductivity and specific heat) are important. The actual response is due to a

complex interaction between the core kinetics, the thermoelectric pump, and the thermal and hydraulic characteristics of the system.

## B. NOMINAL ORBITAL STARTUP

### 1. Startup Conditions

The nominal startup conditions are (Reference 2):

Orbit	700 mile elliptical orbit
Source Level	$10^{-11}$ kw
Drum Repetition Time	150 sec
Initial Flow Rate	4.92 lb/min, 6% of full flow
Initial Temperature	70°F

For purposes of analysis, the following core parameters are established as nominal:

Fuel Temperature Coefficient	$-(0.075 + 5.7 \times 10^{-5} \bar{T}_f) \text{ } \epsilon / ^\circ\text{F}$
Grid Plate Coefficient (each plate)	$-(0.065 + 2.5 \times 10^{-5} \bar{T}_{gp}) \text{ } \epsilon / ^\circ\text{F}$
Overall Thermal Conductance, UA (Figure 10)	

The power, flow, and inlet and outlet temperatures during the initial power transient (i.e., first penetration into power range) are shown in Figure 11. These curves span a 240-sec period during which the power peaks at 43 kw and the flow rate at 42 lb/min, 60 sec later than the power. Because of the long system time constant at low flow rates, the inlet temperature does not respond to the reactor transient until the maximum flow rate is passed.

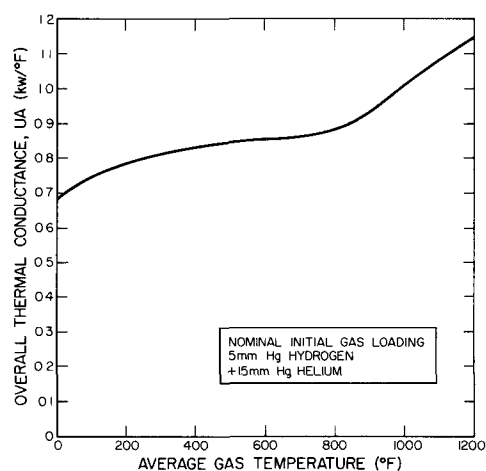
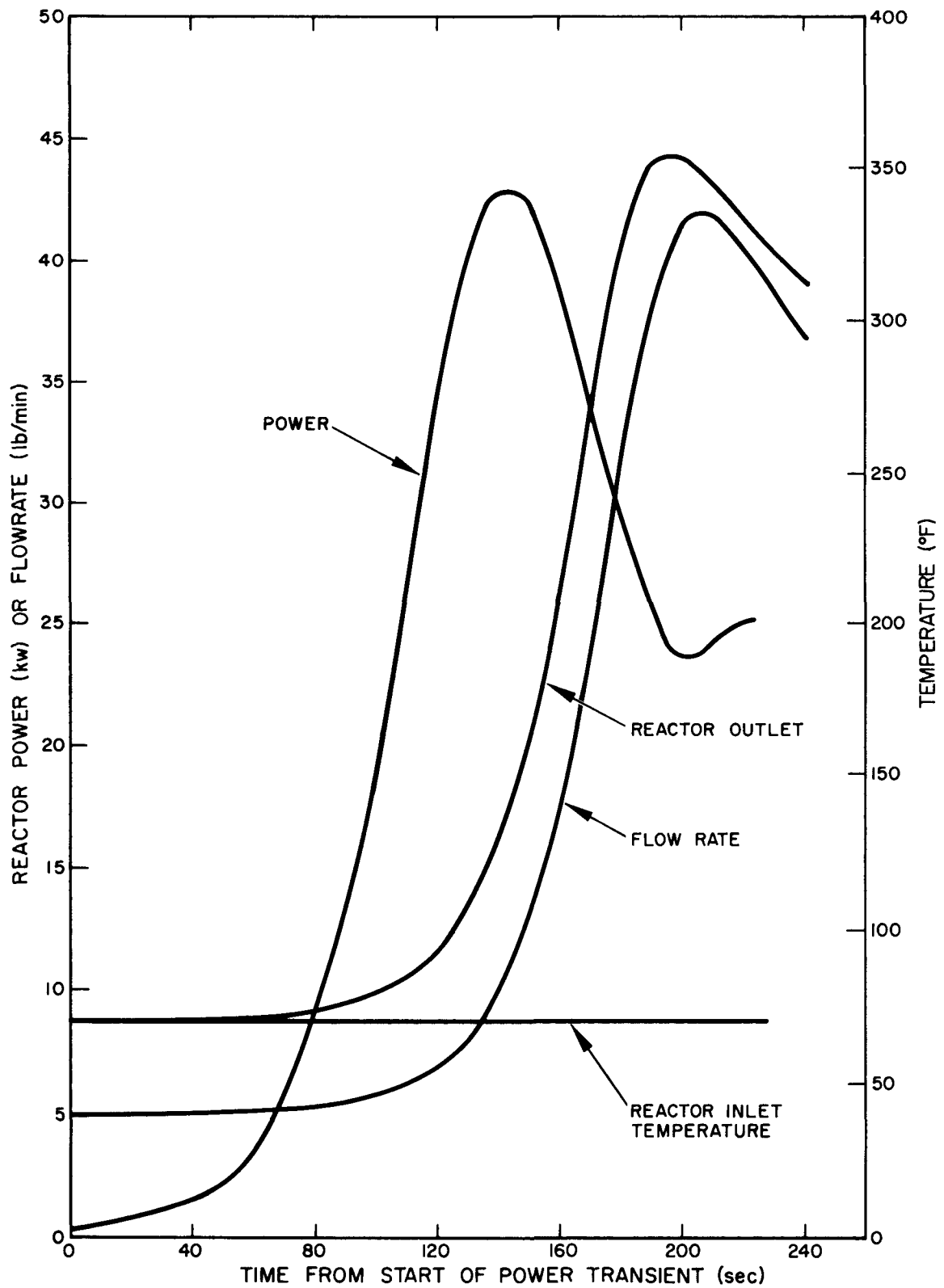


Figure 10. Overall Thermal Conductance UA for SNAP 10A Reactor



6-16-64

7623-0367

Figure 11. Reactor Power, Flow Rate, Inlet and Outlet Temperature During Initial Power Transient

## 2. Temperature During Initial Power Transient

To evaluate thermal stresses within the fuel rods, transient radial temperature distributions have been determined for the first 240 sec of the power transient. Highest thermal gradients occur 5-1/2 in. from the lower end of the center fuel rod; the corresponding radial temperature distributions are plotted in Figure 12. The temperature gradient increases to a maximum 60 sec after peak power and thereafter decreases. The peak fuel stress occurs at the fuel surface where the temperature is lowest. Tangential stress at this point is 960 psi, well below the ultimate tensile strength of the fuel ( $\sigma_t > 15,000$  psi at the local temperature).

The fuel-to-clad temperature excess in the center fuel element reaches a maximum 50 sec after the power peaks. At this time, and at a point 6 in. from the lower end of the fuel rod, the difference between the local fuel and the adjacent clad temperatures on the center element reaches a maximum of 80°F (407 to 327°F) as shown in Figure 13. At this time, the difference between the axial average fuel and clad temperatures on the centerline fuel element is 38°F (344 to 306°F) as compared to the steady-state difference of 29°F.

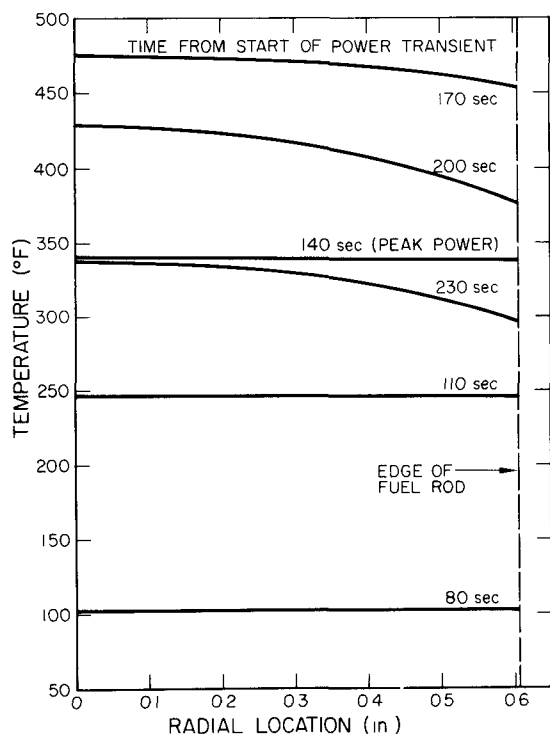


Figure 12. Radial Temperature Profiles in Center Fuel Element at 5-1/2-Inch Elevation During Initial Power Transient

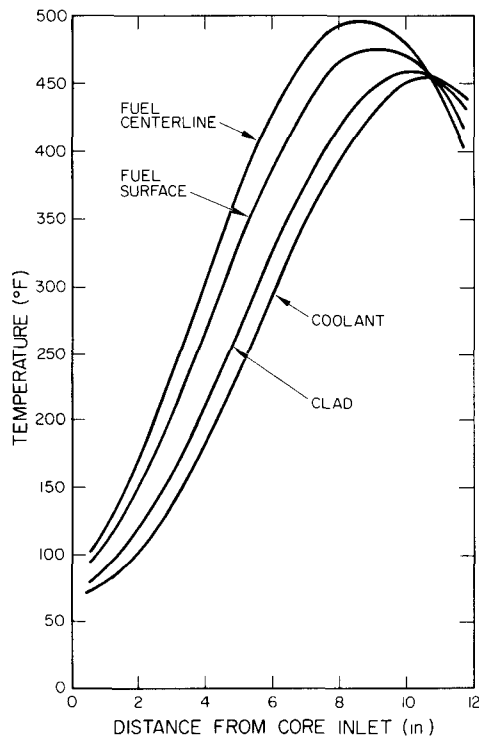


Figure 13. Axial Temperature Profiles  
in Center Fuel Element 50 Seconds  
After Peak Transient Power

6-16-64

7623-0369

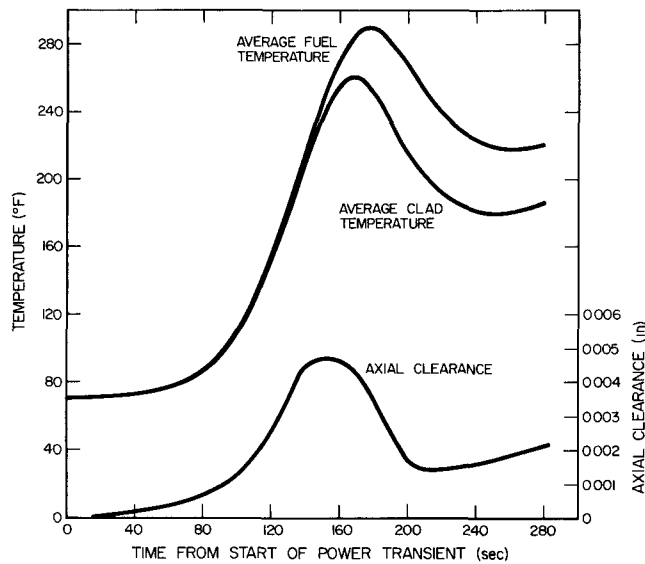
Average fuel and clad temperatures are plotted in Figure 14 for the core average element and in Figure 15 for an element at the edge of the core. The axial clearance between the fuel and the upper end cap is also plotted for these two cases. No axial interference occurs during the transient; the minimum clearance is 1.0 mil, 80 sec after peak power. Because of the thermal expansion characteristics of the fuel and the cladding material, clearances are somewhat less at the edge of the core than they are at the average radial position.

Throughout startup and during steady-state operation, temperatures of the hydrogen barrier and the Hastelloy N clad differ by no more than 7°F. This can be shown by using a peak heat flux of 15,200 Btu/hr-ft<sup>2</sup> corresponding to the 43-kw peak power during startup. For this heat flux, the temperature difference between the inside surface of the 0.004-in. (maximum) thickness of barrier coating and the outer surface of the 0.0155-in. (maximum) clad thickness is:

$$T = \frac{Q}{A} \sum \frac{\Delta X}{k}$$

$$= 15,200 \left( \frac{.0155}{10.9(12)} + \frac{.004}{1(12)} \right) = 6.9^{\circ}\text{F}$$

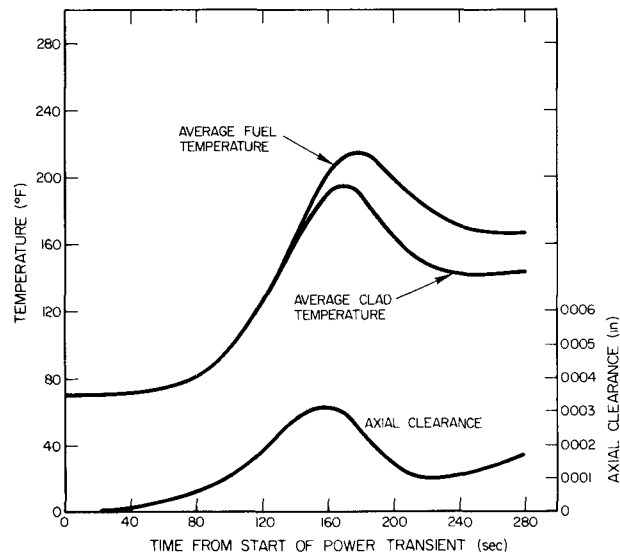




6-16-64

7623-0370

Figure 14. Average Temperatures and Axial Clearances for Core Average Element During Initial Power Transient



6-16-64

7623-0371

Figure 15. Average Temperatures and Axial Clearances for Core Edge Element During Initial Power Transient

The difference between the mean barrier and the mean clad temperature does not exceed 4°F.

A relatively severe temperature gradient exists during startup at the junction of the Hastelloy N clad and the upper end cap. The difference between the average end cap temperature and the clad temperature 0.1 in. below the end cap reaches a maximum of 72°F in the centerline fuel rod 30 sec after the transient power peak (Figure 16).

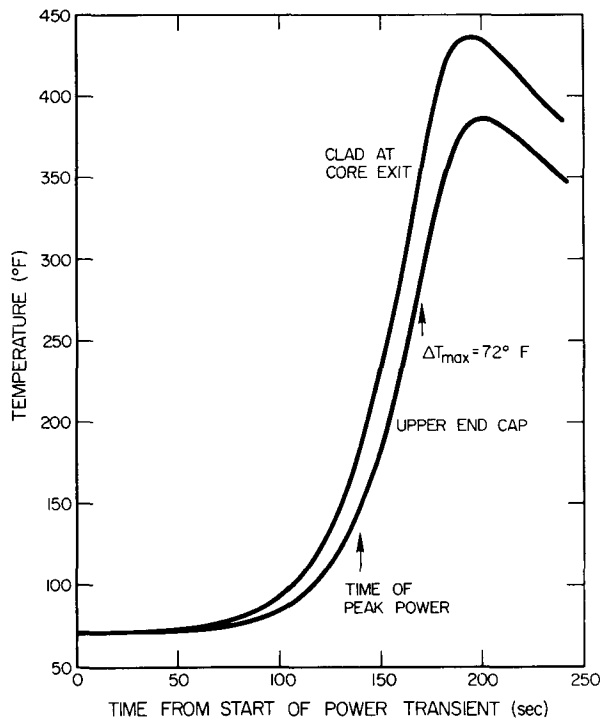


Figure 16. Upper End Cap and Clad Temperatures in Center Element During Initial Power Transient

6-16-64

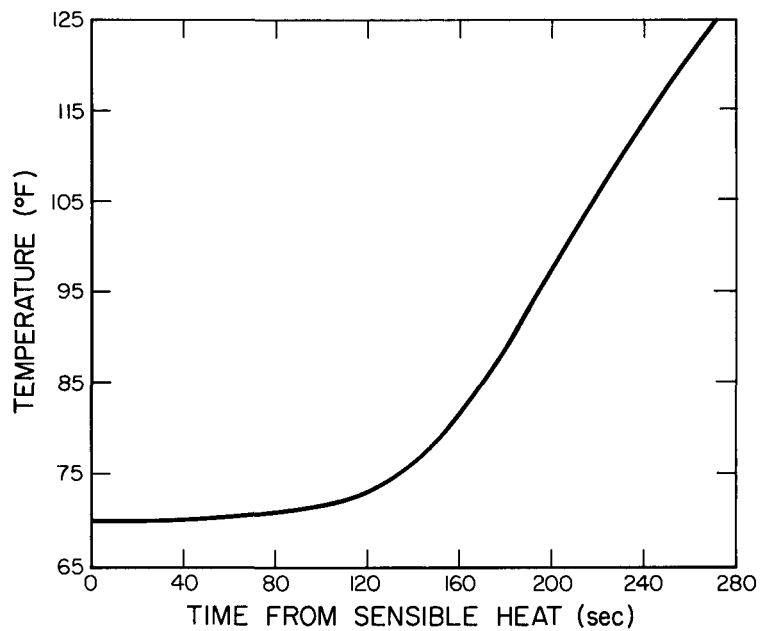
7623-0372

As shown in Figure 17, the beryllium internal reflectors heat slowly throughout the initial power transient, and the temperature gradients within the reflectors are slight. The axial profile at the time of maximum core outlet temperature (200 sec after sensible heat) is plotted in Figure 18; the maximum temperature variation is less than 40°F.

### 3. Differential Fuel-Clad Expansion

The maximum fuel-to-clad temperature difference occurs 50 sec after the initial power peak when the average fuel temperature in the center fuel element is 407°F and the clad temperature is 327°F.

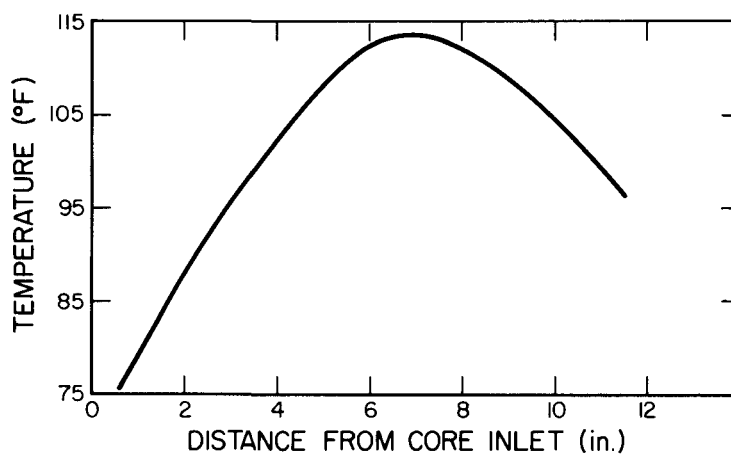
This is the most severe local condition in the core, occurring 6 in. from the lower end of the fuel rod. These temperatures produce a net increase in the



6-16-64

7623-0373

Figure 17. Average Internal Reflector  
Temperatures During Initial  
Power Transient



6-16-64

7623-0374

Figure 18. Internal Reflector Temperatures  
at Time of Maximum Core Outlet  
Temperature

diametric fuel-clad clearance of 0.0004 in. The minimum axial fuel-clad clearance during startup occurs on the edge fuel element and is 0.0010 in. (Figure 15).

#### 4. Differential Clad-Hydrogen Barrier Expansion

Because the temperature excess of the hydrogen barrier over the adjacent clad will not exceed 7°F during the life of SNAP 10A, the assumption of equal clad and barrier temperatures can be applied in determining the differential expansion at any point in the fuel element.

The combination of softening temperature of the barrier and operating temperatures in the fuel element produces compression in the barrier during fabrication and relaxation of barrier stresses between launch and operating temperatures. The prestress diminishes during startup, reaching a minimum at the steady-state temperature levels in orbit. The final temperatures are below the softening temperature of the barrier material and well below the range in which crystallization takes place.

#### 5. Thermal Stresses in Clad and Barrier at Junction to Upper End Cap

The Hastelloy-N clad and the ceramic barrier are subject to maximum tensile stresses at the junction of the upper end cap and the clad. These stresses are related to the difference between the average end cap temperature and the adjacent clad temperature. As noted in Section IV-B-2, the maximum temperature difference between the end cap and clad 0.1 in. from the cap occurs in the center element and is 72°F (Figure 16). The corresponding maximum tensile stresses in the clad and the barrier are 28,700 and 9,600 psi, respectively.

The yield strength of Hastelloy-N is 40,000 psi at 500°F. This assures an adequate margin of safety for the clad. Because of the bonding procedure used, a residual compressive stress of approximately 25,000 psi exists in the barrier when the element is heated to 400°F during startup. Therefore, the barrier remains in compression throughout startup.

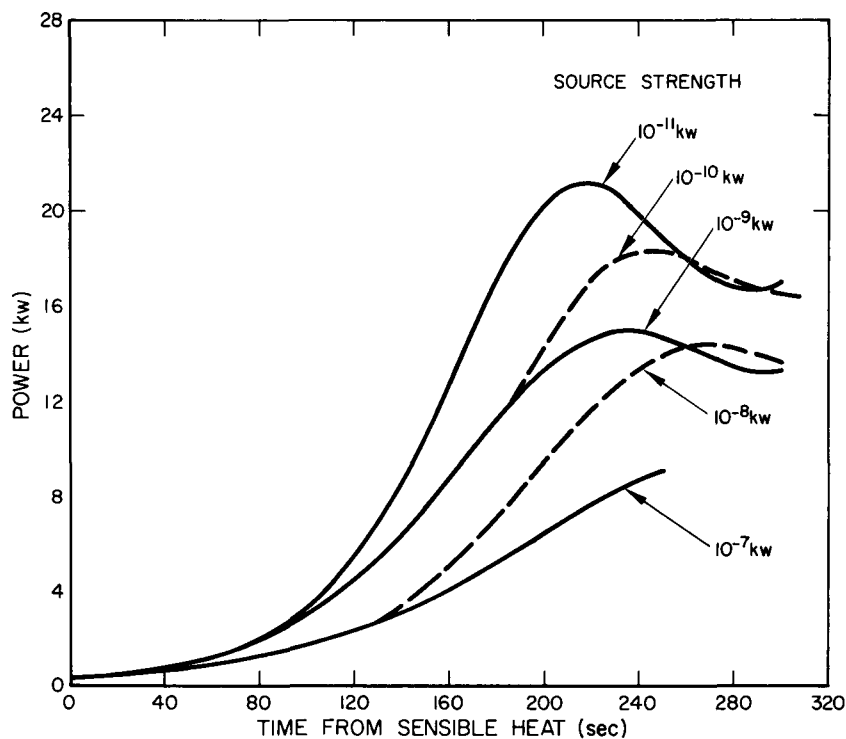
#### 6. Thermal Stresses in Clad and Barrier at Junction to Lower End Cap

Discontinuity stresses at the bottom of a fuel element, where the blend cup, barrier and clad are in contact, are induced by the differences in thermal expansion between the cylindrical sides of the cladding and the lower end cap. During the startup transient, these stresses are always less than the corresponding stresses at the junction to the upper end cap. Consequently, the barrier stress is always less than the precompression of the barrier material.

### C. STARTUP OF FS-1 GROUND TEST SYSTEM

Two preliminary startups precede the normal startup sequence on the 10FS-1 ground test. The first employs a fine control drum stepping period of 300 sec, twice the nominal period. This test is terminated after the initial power peak, the total time in the power range (above sensible heat) being less than 30 min. The second preliminary test employs the design stepping rate of 150 sec, but is also terminated after the initial power transient. During these two tests, the maximum fuel temperature in the core will not exceed 520°F. After the preliminary tests, and presuming the reactor functions as predicted, a normal startup leading to steady-state operation will be undertaken.

To assist in the evaluation of 10FS-1 startup, the effect of source strength on the startup transients was determined. Source strength was varied by decades from  $10^{-11}$  to  $10^{-8}$  kw. A drum stepping rate of 300 sec, an initial reactor temperature of 70°F, and an initial flow rate of 4.92 lb/min were assumed in each case. The results are summarized in Figures 19, 20 and 21 where power, reactor outlet temperature and flow rate are plotted, respectively.



6-16-64

7623-0375

Figure 19. Effect of Source Strength on Power Transient During FS-1 Startup



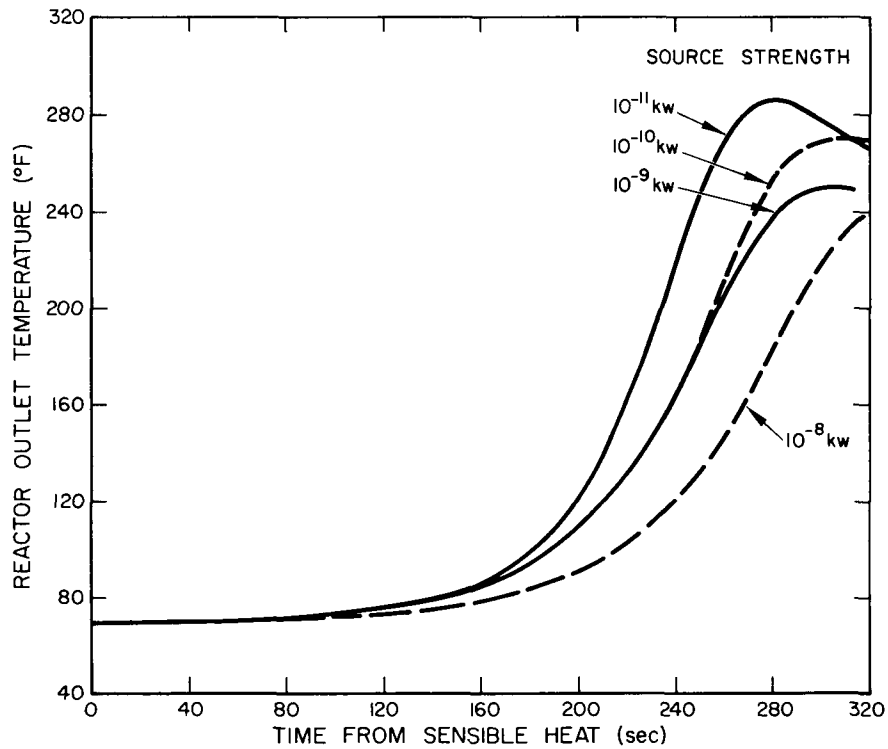


Figure 20. Effect of Source Strength on  
Outlet Temperature Transient  
During FS-1 Startup

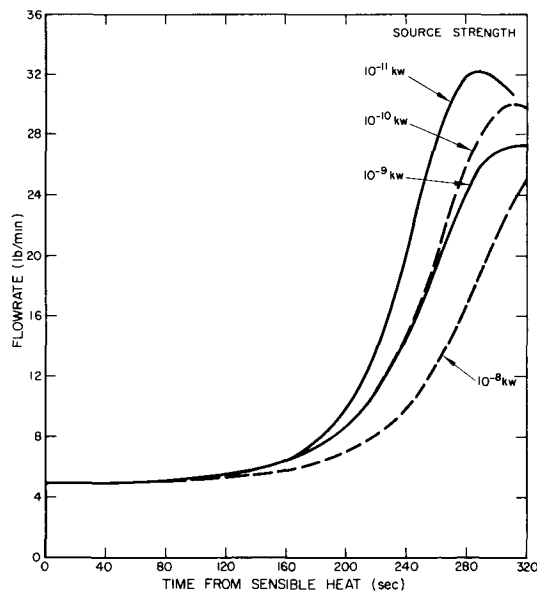


Figure 21. Effect of Source Strength on  
Flow Rate Transient During  
FS-1 Startup

The nominal equivalent multiplied source strength is  $10^{-9}$  kw, furnished by a 1.25 curie source inserted in the FS-1 system. The minimum possible source level,  $10^{-11}$  kw, is that provided by spontaneous fissions within the core.

The primary parameter affecting startup is the excess reactivity inserted before the initial power peak. In general, the larger the source, the smaller will be the reactivity inserted (fewer drum steps) prior to peak power and the weaker the transient. Increasing the source level reduces the time required to achieve power operation. Thus, with a fixed drum stepping rate, fewer steps are taken before the initial power peak, and the excess reactivity is correspondingly decreased. This behavior is illustrated in Figure 19 where the power transients determined for the four source levels are plotted. The larger power transients produced by the weaker sources result in more severe reactor outlet temperature and flow rate transients (Figures 20 and 21). Maximum rates of change are shown in Table 5.

TABLE 5  
SUMMARY OF FS-1 STARTUP CONDITIONS  
AS FUNCTIONS OF SOURCE STRENGTH

Source Strength (kw)	Maximum Power (kw)	Maximum Rate of Change Outlet Temperature ( $^{\circ}$ F/sec)	Maximum Rate of Change Flow Rate (lb/min-sec)
$10^{-11}$	21.2	3.1	0.37
$10^{-10}$	18.4	2.4	0.31
$10^{-9}$	15.0	2.0	0.26
$10^{-8}$	14.4	1.8	0.24

#### D. OFF-DESIGN STARTUP CONDITIONS

Table 6 summarizes the maximum thermal stresses anticipated for various SNAP 10A startup conditions. The cases reported are:

- 1) Nominal startup, 23.6¢ excess reactivity — this is the nominal case discussed in Section IV-B. The uncertainty in excess reactivity is one drum step or approximately three cents.
- 2) Nominal startup with Hastelloy-C grid plates — this is identical to the preceding case except for (1) temperature coefficients corresponding to Hastelloy-C grid plates and (2) an earlier drum worth curve.

TABLE 6  
CONDITIONS OF MAXIMUM SEVERITY ENCOUNTERED  
DURING FIRST TRANSIENT PULSE

	1 <sup>†</sup>	2	3	4	5	6	7	8	9	10
	Nominal SS Grid Plates Rev Drum Worth	Hastelloy C Grid Plates	Additional Drum Step	Rapid Drum Step	Rapid Drum Step	Slow Drum Low Source	Slow Drum High Source	Zero Initial Flow	Low $\alpha_f$ (1/2 nom )	Low UA (1/2 nom )
Drum stepping rate (sec)	150	150	150	50	100	300	300	150	150	150
Source strength (kw)	$10^{-11}$	$10^{-11}$	$10^{-11}$	$10^{-11}$	$10^{-11}$	$10^{-11}$	$10^{-8}$	$10^{-11}$	$10^{-11}$	$10^{-11}$
Time to sensible heat (hr)	6 69	6 15	6 15	2 12	4 15	12 14	12 05	6 15	6 15	6 15
Excess reactivity (cents)	24 0	23 6	26 5	38 0	29 7	17 4	14 3	23 6	23 6	23 6
Peak power (kw)	43 0	42 0	56 2	127	63 5	21 1	14 4	43 8	64 2	49 1
Maximum fuel tempera- ture (°F)	498	511	600	778	586	356	256	632	615	717
Maximum outlet tempera- ture (°F)	354	371	420	550	435	286	246	466	450	635
Maximum rate of change of outlet temperature (°F/sec)	6 7	6 9	9 2	16 8	9 5	3 3	1 9	10 4	10 6	8 9
Maximum flowrate (lb/min)	42 0	44 1	50 3	68 0	52 5	32 2	26 6	49 4	55 0	46 5
Maximum fuel stress (ksi)	0 96	1 09	1 55	2 64	1 34	-	-	1 75	1 74	-
Maximum clad stress (ksi)	28 7	26 7	31 9	46 5	34 1	-	-	40 3	34 5	37 3
Minimum barrier com- pressive stress (ksi)	15 4	16 1	14 6	9 9	14 0	-	-	11 7	13 8	13 1
Minimum axial clearance (mils)		1 0	0 7	-1 0 (interfer- ence)	0 7	-	-	0 7	0 7	0 5

Center channel (power generation rate 31% greater than core average)

<sup>†</sup>Case 1 assumes stainless-steel grid plates all others Hastelloy C

Case 2 employs a revised drum worth curve

- 3) Increased reactivity, one additional drum step – identical to case 2 except for increased reactivity produced by added drum step.
- 4) Fast drum stepping rate, once every 50 sec.
- 5) Fast drum stepping rate, once every 100 sec.
- 6) Slow drum stepping rate, once every 300 sec.
- 7) Slow drum stepping rate with increased source strength ( $10^{-8}$  kw rather than  $10^{-11}$  kw).
- 8) Zero coolant flow at initiation of startup.
- 9) Reduced fuel temperature coefficient, one-half nominal.
- 10) Reduced overall thermal conductance UA, one-half nominal.

The tabulation provides information on the effect of varying excess reactivity, drum stepping rate and source strength. The most important parameter affecting the startup transient is the excess reactivity: the reactivity added between criticality and sensible heat. Changes in drum stepping rate and source strength produce changes in excess reactivity and thus indirectly modify the startup transient.

## E. TRANSIENT LIMITATIONS UPON STARTUP

### 1. Barrier Stress Limitation

The most probable mode of core failure during 10A startup is cracking of the ceramic hydrogen barrier at the junction of the upper end cap and the cladding. Due to the residual compressive stress of 25,000 psi (at 400°F) within the barrier, a maximum tensile stress of approximately 35,000 psi, corresponding to a resultant tensile loading of 10,000 psi, can be applied to the barrier before cracking occurs.

The most severe startup barrier conditions occur during the flow transient which follows the initial power peak. During this time, the temperature gradient along the cladding is essentially proportional to the clad-to-end cap temperature difference, and the barrier stress can be directly related to this temperature difference by the approximate equation:

$$\sigma_b = 2.08 E_b \alpha_c \Delta T$$

where

$\sigma_b$  = barrier tensile stress, 35,000 psi maximum

$E_b$  = barrier modulus of elasticity,  $10 \times 10^6$  psi

$\alpha_c$  = clad coefficient of thermal expansion,  
 $6.45 \times 10^{-6}$  in./in. °F

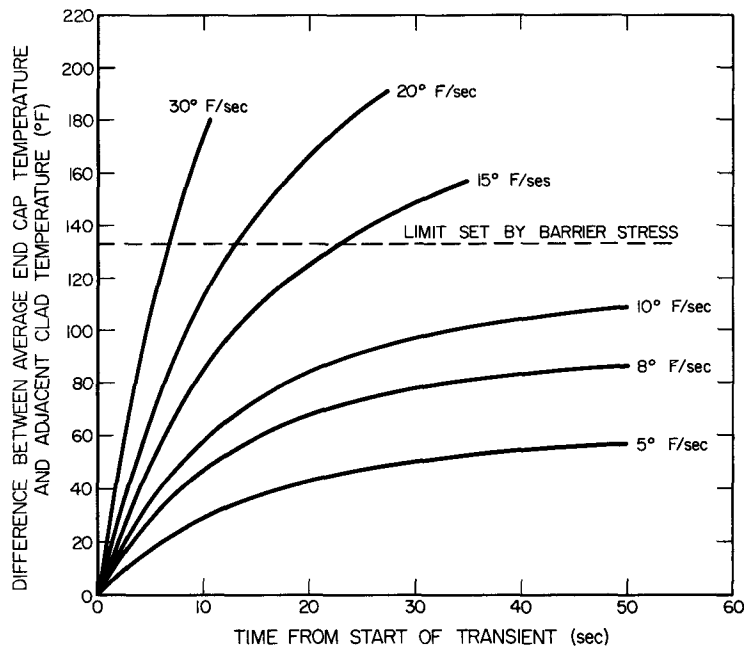
$\Delta T$  = clad-end cap temperature difference, °F

Consequently, the maximum tolerable temperature difference is 260°F.

The most severe stresses occur within the centerline fuel element which has an internal heat generation rate 31% greater than that of the core average. When a clad-to-end cap temperature difference of 260°F is induced on the center element, the corresponding temperature difference on the core average element is approximately 23% less or 200°F. If a safety factor of 1.5 is assumed, the maximum tolerable temperature difference on the core average element is 133°F.

## 2. Maximum Duration of Outlet Temperature Transients

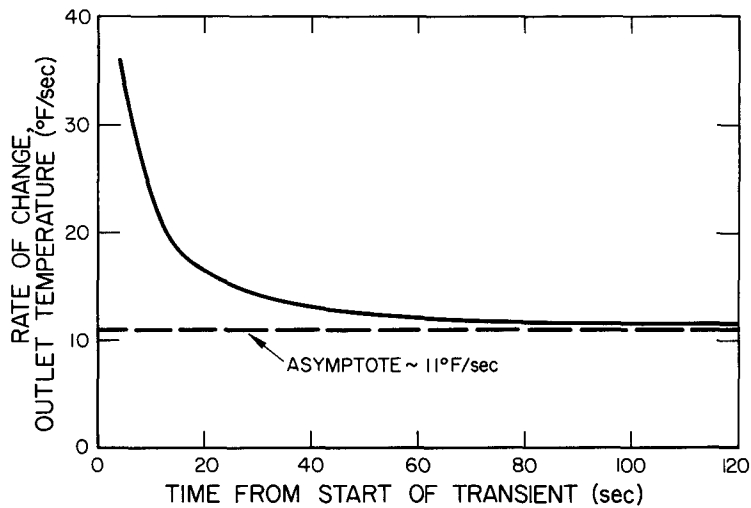
This temperature difference has been related to the severity and the duration of the reactor outlet temperature transient. The clad-to-end cap temperature difference is plotted as a function of the transient duration in Figure 22, and the maximum allowable durations for the outlet temperature transient are shown in Figure 23. Because of the 133°F limit, the more severe transients can be tolerated for only limited times: a 30°F/sec transient for 6.7 sec, a 20°F/sec transient for 13.1 sec, and a 15°F/sec transient for 23 sec. Transients of 11°F/sec or less will never crack the barrier regardless of how long they are sustained. (However, limits are eventually set by temperatures reached within the core or by axial interference between the fuel and the upper end cap.)



6-16-64

7623-0378

Figure 22. Clad-End Cap Temperature Difference During Outlet Temperature Transients



6-16-64

7623-0379

Figure 23. Maximum Rate of Change of Outlet Temperature as Function of the Duration of the Transient

4/2

## REFERENCES

1. G. M. Anderson, "Nuclear Reactor Systems," *Astronautics and Aerospace Engineering*, Vol. 1, No. 4, (May 1963) pp 27-36
2. G. S. Drucker and T. J. Boyle, "SNAP 10A In-Orbit Prestart and Startup," NAA-SR-9720 (1964)

BLANK



**APPENDIX A**  
**CORE MATERIALS AND PHYSICAL PROPERTIES AT 950°F**

	Material	Density (lb/ft <sup>3</sup> )	Specific Heat (Btu/lb °F)	Conductivity (Btu/hr-ft °F)
Internal reflectors	Be	113	0.65	63
Grid plates	316 SS	495	0.135	11
Fuel	ZrH + 10 wt % U	350	0.15	13
Fuel element cladding	Hastelloy-N	538	0.10	10.9
Diffusion barrier	Ceramic	140	0.20	1
Coolant	NaK-78	46.8	0.209	15
Gas gap	H <sub>2</sub> + 15 mm He			0.20

Vapor pressure of NaK at 1000 °F (psia) 0.8

Vapor pressure of NaK at 1100 °F (psia) 1.7

## APPENDIX B

### COMPUTER CODES USED IN EVALUATING THERMAL PERFORMANCE

The analytic results summarized in this report were obtained by the use of three digital computer codes:

- 1) HEAP: Hot-channel effects
- 2) TRANCORE: Single element transient temperatures
- 3) CORESECT: Core transient temperatures.

The Hot-Element Analysis Program (HEAP) incorporates various hot-channel factors to calculate steady-state fuel, gas gap, barrier, clad and coolant temperatures for the core hot element. If all hot-channel factors are set equal to one, HEAP determines the nominal steady-state temperature distributions within a fuel element; the radial location of the element is set by the assumed radial power factor.

Transient temperatures are calculated by the TRANCORE and CORESECT codes. Both codes are divided into three routines:

- 1) Core heat transfer
- 2) Reactor kinetics, and
- 3) Thermoelectric pump

The two codes differ only in the thermal model; CORESECT simulates the repeating one-twelfth section of the reactor core, and TRANCORE simulates one fuel element with its associated coolant. Consequently, the former code provides an overall picture of temperatures within the reactor while the latter presents more detailed information on an individual element.

The three thermal codes are discussed in greater detail in the following sections, and the appendix concludes with the specific application of the codes to the SNAP 10A reactor.

#### 1. THE HOT-ELEMENT ANALYSIS PROGRAM: HEAP

The Hot-Element Analysis Program (HEAP) considers a tricuspid coolant channel, defined as the hot channel, and the three fuel elements adjoining it, one of which is the hot element. All coolant channels receiving heat from the three elements, other than the hot channel, are considered to have the same axial temperature distribution, i. e., a nominal distribution calculated by the code on the basis of input data for core power distribution, core power, and coolant flow.

The code subdivides this model axially into 100 equal increments. The program then determines an energy balance and the temperatures at the downstream end of each of the increments. The following hot-channel factors are used in the analysis:

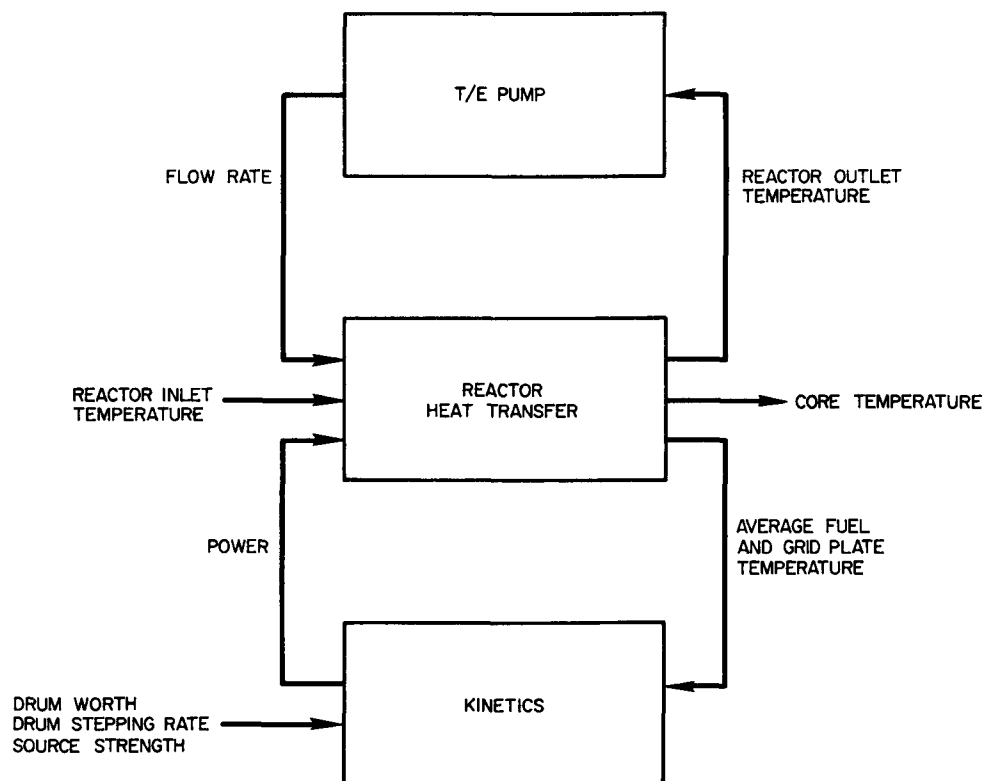
- a)  $F_H$ : The ratio of the maximum effective local surface film thermal resistance to the average surface film resistance; this factor is introduced to evaluate the effect of circumferential variation in heat flux and heat-transfer coefficient, resulting from the local variation of coolant velocity in a tri-cuspid channel. The factor may also be used to obtain the temperature difference across the clad and/or barrier.
- b)  $F_P$ : The ratio of element maximum power to nominal power; this factor is used to account for the effect of uncertainty in fuel element composition.  $F_P$  may also include the effect of uncertainty in reactor power distribution, but a preferred method of accounting for this is modification of the input value for nominal power.
- c)  $F_Q$ : The ratio of overall radial thermal conductance between the point of maximum fuel temperature and the hot channel to the nominal radial conductance. The nominal radial conductance is defined as the overall conductance between fuel centerline and coolant for a fuel element with azimuthally uniform heat flux. This factor is designed to duplicate the effect of eccentricity of the fuel within the fuel element assuming that the fuel touches the barrier adjacent to the hot channel.
- d)  $F_W$ : The ratio of nominal to minimum coolant flow in the hot channel. This factor is used to determine the effect of local flow deficiency due to imperfect orifice design and construction. It is assumed that no coolant mixing occurs between the hot channel and adjacent channels.

The hot-channel factors  $F_H$  and  $F_Q$  are evaluated by studies of detailed temperature distributions in a fuel element and coolant channel. These studies generally use a nodal network analysis code, such as TIGER (Temperatures from Internal Generation Rates) or TAP (Thermal Analyzer Program).

## 2. TRANSIENT CODES - TRANCORE AND CORESECT

To simulate transient behavior of the SNAP 10A reactor, the two digital computer codes, TRANCORE-10A and CORESECT-10A, were prepared. The codes are used to determine transient temperatures and, subsequently, thermal stresses within the reactor core. In addition, the codes predict power, flow and reactor inlet and outlet temperatures. The codes can be used to investigate a wide variety of reactor operational behavior: steady-state, startup, scram, loss of coolant flow, etc. However, they cannot evaluate the effects of rapid reactivity changes, i.e., operation near prompt critical.

Both codes are divided into three routines: core heat transfer, reactor kinetics and thermoelectric pump. A schematic of the basic common code, indicating the various inputs and outputs of each of the three routines, is shown in Figure 24. As one would anticipate, the three sections are interrelated: core temperatures are dependent on reactor power, flow rate and inlet temperature; power is dependent on average fuel and grid plate temperatures; and flow rate is dependent on reactor outlet temperature.



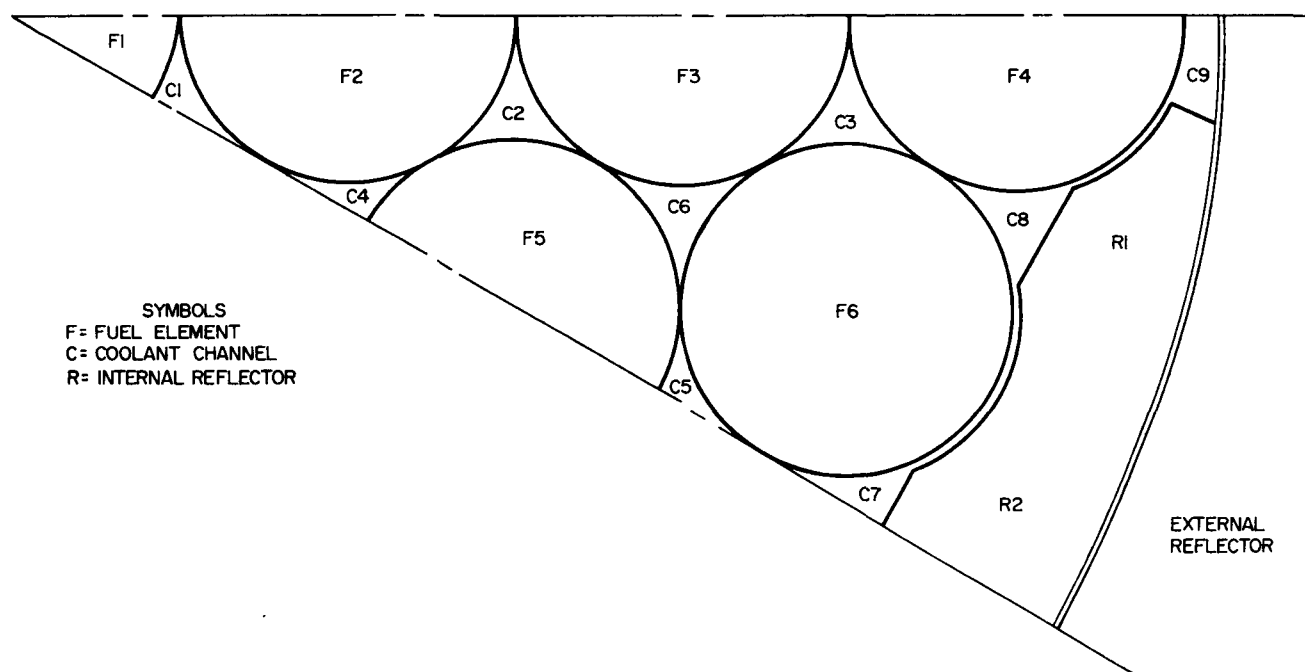
6-16-64

7623-0380

Figure 24. Block Diagram of TRANCORE and CORESECT Transient Temperature Codes

The TRANCORE heat-transfer routine, using the physical constants associated with the 10A reactor, calculates temperatures for one or two fuel elements within the core. The thermal model considers an element with its associated lower and upper end caps, lower and upper grid plates, surrounding coolant and the two plenums. The fuel element is divided into five radial and ten axial sections to give a fifty-node representation. Depending upon the radial power factor used, the model is representative of fuel elements at various radial locations within the core. Ten coolant nodes are employed, at axial positions identical to those of the fuel nodes. The associated upper end cap and grid plate are each divided into five radial nodes, matching those of the fuel elements. The mean temperature of the fifty fuel nodes is taken as the average fuel temperature. An average coolant temperature is similarly determined from the ten coolant node temperatures. Average upper and lower grid plate temperatures are calculated for use with the kinetics routine.

The CORESECT thermal model simulates the repeating 1/12 section of the reactor core (Figure 25). The core section, which is subdivided axially into 10 planes, contains 1 complete fuel element, 5 partial elements, 4 complete coolant channels, 4 half-channels, 1/2 an internal reflector, 1/2 an edge channel,



6-16-64

7623-0381

Figure 25. CORESECT Core Thermal Model

and 1/12 of the vessel wall and the external reflector structure. Axial conductance within the fuel elements, internal reflector, stagnant coolant channel, vessel wall and external reflector is considered. Various flow distributions are duplicated by program options:

- a) equal mass velocity in each orificed channel and stagnant coolant in the edge (unorificed) channel
- b) equal mass velocity in all channels, including the edge channel
- c) axially variable mass flow in each channel due to crossflow between channels

Crossflow effects must be determined separately and introduced as inputs into CORESECT. The greatest usefulness of the CORESECT thermal model is its predictions of temperatures near the edge of the core where the internal reflectors and the edge channels must be considered.

The reactor kinetics routine used in both codes simulates the nuclear behavior of the reactor and calculates power as a function of time. External inputs required are drum worth, drum stepping rate, source strength, and shutdown reactivity. In addition, the core average fuel and grid plate temperatures calculated by the heat-transfer routines are used in the determination of reactivity changes.

The thermoelectric pump, located above the reactor on the coolant exit line, consists of three major components:

- a) A dc electromagnetic liquid-metal pump
- b) Two positive and two negative thermoelectric elements, and
- c) Four heat-radiating fins.

Heat flow is from the relatively hot NaK in the throat of the pump out through copper conductors and the thermoelectric elements and along the fins which radiate to space. The imposed temperature differences across the thermoelectric elements generate a dc voltage by the Seebeck effect. This voltage sets up a current through the NaK at right angles to the field of the attached permanent magnet. The resulting electromagnetic interaction produces a force within the NaK, driving the liquid metal through the pump and around the system loop.

The computer simulation is accomplished by solving finite-difference approximations to the basic pump equations. Thus, the instantaneous coolant flow rate is calculated. Required inputs to the pump routine are the reactor outlet temperature and the equivalent space temperature.

### 3. APPLICATION OF CODES TO SNAP 10A REACTOR

Nominal steady-state temperature distributions for the core average and center element were calculated with the HEAP and TRANCORE codes and checked with CORESECT; the agreement between the three codes is excellent. Edge element (marked as No. 4 in Figure 25) and internal reflector temperatures were determined by CORESECT.

The following hot-channel factors were used in the HEAP code to calculate hot-element temperatures:

- a)  $F_H = 2.0$
- b)  $F_P = 1.03$  for two elements bordering the hot channel, 1.00 for the third
- c)  $F_Q = 1.20$  for two elements bordering the hot channel, 1.00 for the third
- d)  $F_W = 1.00$  (uniform radial flow distribution).

Temperature distributions during the nominal startup transient were determined by TRANCORE and CORESECT. Temperatures, power and flow rate as functions of time are in excellent agreement. TRANCORE was used to determine all other startup transients.